Geochimica et Cosmochimica Acta 338 (2022) 165–180

Contents lists available at ScienceDirect

Geochimica et Cosmochimica Acta

journal homepage: www.elsevier.com/locate/gca

The cadmium and zinc isotope compositions of the silicate Earth – Implications for terrestrial volatile accretion

Harvey Pickard [a,1], Emeliana Palk [a,b], Maria Schönbächler [c], Rebekah E.T. Moore [a], Barry J. Coles [a], Katharina Kreissig [a], Katrina Nilsson-Kerr [d,2], Samantha J. Hammond [d], Eiichi Takazawa [e], Christophe Hémond [f], Peter Tropper [g], Dan N. Barfod [h], Mark Rehkämper [a,*]

[a] Department of Earth Science & Engineering, Imperial College London, London SW7 2AZ, UK
[b] School of Earth Sciences, University of Bristol, Bristol BS8 1RJ, UK
[c] Department of Earth Sciences, ETH Zürich, Clausiusstrasse 25, 8092 Zürich, Switzerland
[d] School of Environment, Earth and Ecosystem Sciences, The Open University, Milton Keynes MK7 6AA, UK
[e] Department of Geology, Niigata University, 2-8050 Ikarashi, Nishi-ku, Niigata 950-2181, Japan
[f] Université de Bretagne Occidentale Brest, CNRS, Ifremer, Geo-Ocean, UMR6538, 29280 Plouzane, France
[g] Institute of Mineralogy and Petrography, University of Innsbruck, Innrain 52f, 6020 Innsbruck, Austria
[h] Scottish Universities Environmental Research Centre, Rankine Avenue, Scottish Enterprise Technology Park, East Kilbride G75 0QF, Scotland, UK

ARTICLE INFO

Article history:
Received 26 November 2021
Accepted 29 September 2022
Available online 6 October 2022
Associate editor: Frederic Moynier

Keywords:
Isotope geochemistry
Stable isotopes
Volatile elements
Zinc
Cadmium
Silicate Earth
Bulk silicate Earth

ABSTRACT

Zinc and Cd isotope compositions are presented for a comprehensive suite of terrestrial rocks to constrain the extent of Zn and Cd isotope fractionation during igneous processes and better define the δ^{66}Zn and δ^{114}Cd values of the silicate Earth (the δ values denote per mille deviations of ^{66}Zn/^{64}Zn from JMC Lyon Zn and of ^{114}Cd/^{110}Cd from NIST SRM 3108 Cd). Analyses of spinel lherzolites provide a bulk silicate Earth (BSE) $\delta^{114}Cd_{BSE}$ value of –0.06 ± 0.03 ‰ (2SD). For Zn, the peridotite data of the current and previous studies define a mean $\delta^{66}Zn_{BSE}$ = 0.20 ± 0.05 ‰ (2SD). Komatiite analyses of this and published investigations yield similar mean values, which suggests that the Zn and Cd isotope compositions of the mantle remained fairly constant since the Archean. Data for loess provide upper continental crust compositions of δ^{114}Cd = 0.03 ± 0.10 ‰ and δ^{66}Zn = 0.23 ± 0.07 ‰. The Zn isotope and abundance data for peridotites and oceanic basalts are in accord with the previous observation of a mantle array, with basalts having higher Zn concentrations and δ^{66}Zn values than the peridotites. To a first order, this reflects slightly incompatible behaviour of Zn during mantle melting and melt differentiation with associated enrichment of heavy Zn isotopes in the melt phase. Cadmium is marginally more incompatible than Zn during igneous processes and the oceanic basalts also display a minor enrichment of heavy Cd isotopes relative to peridotites. However, secondary processes produce significant Cd isotope variability in both mantle melts and peridotites, obscuring the primary igneous array. The $\delta^{66}Zn_{BSE}$ estimates of this and previous studies resemble the Zn isotope compositions of CV and CO carbonaceous and some enstatite chondrites. In contrast, the BSE has a lower $\delta^{114}Cd_{BSE}$ value than enstatite and carbonaceous chondrites. This implies that the Cd isotope composition of the BSE was either fractionated during accretion or that Earth's Cd inventory was not exclusively acquired from material related to carbonaceous and enstatite chondrites. Importantly, delivery of Zn and Cd to the BSE solely by CI and CM chondrites is not in accord with the meteorite and terrestrial stable isotope data of these elements.

1. Introduction

Despite decades of research, the source of Earth's volatiles, the timing of their accretion and whether the composition of the source materials matches any meteorites within collections are still topics of considerable debate. This uncertainty encompasses both moderately volatile elements, such as Na, Mn and Cu, with 50 % condensation temperatures (T_C) of between about 1300 K

* Corresponding author.
E-mail addresses: hpic@bgs.ac.uk (H. Pickard), markrehk@imperial.ac.uk (M. Rehkämper).
[1] Now at National Environmental Isotope Facility, British Geological Survey, Keyworth, Nottingham NG12 5GG, UK.
[2] Now at Department of Earth Sciences, University of Bergen, Bergen 5007, Norway.

https://doi.org/10.1016/j.gca.2022.09.041
0016-7037/

and 700 K, and more volatile species, such as water and Cl, that condense at lower temperatures (Albarède, 2009; Wood et al., 2010). Notably, both the Earth and chondritic meteorites exhibit variable depletions in volatile constituents, which are generally correlated with an element's volatility, but display refractory element abundance ratios similar to those of the bulk Solar System, as approximated by the Sun and CI carbonaceous chondrites (Wasson and Chou, 1974; Wasson and Kallemeyn, 1988; McDonough and Sun, 1995; Palme et al., 2014; Palme and O'Neill, 2014).

Considering Earth's accretion history, many studies argue for volatile accretion during the main stages of accretion, whilst core formation was ongoing. Specifically, it was posited that oxidised, volatile-rich material was added during the later stages of accretion to an initially refractory and volatile-depleted proto-Earth (Wänke et al., 1984), with progressive oxidation of the mantle supported by continuous core formation models (Wade and Wood, 2005; Corgne et al., 2008; Siebert et al., 2011). Accretion of carbonaceous material equating to ≤15 % of Earth's mass during the later stages of accretion was thereby considered to satisfy both isotopic constraints (Schönbächler et al., 2010) and terrestrial volatile element abundances (Marty, 2012; Albarède et al., 2013; Braukmüller et al., 2019). Alternatively, the close genetic relationship between Earth and enstatite chondrites in mass independent isotope compositions of O and various metals (including Ca, Ti, Cr, Ni, Mo, Ru, Nd), suggests that the latter may be the primary source of Earth's volatile inventory (Javoy et al., 2010; Warren, 2011; Burkhardt et al., 2011; Young et al., 2016; Dauphas, 2017; Fischer-Gödde and Kleine, 2017; Bermingham et al., 2018; Boyet et al., 2018; Gillmann et al., 2020). This is supported by data, which demonstrate that enstatite chondrites could have supplied Earth's water budget whilst also satisfying constraints from H and N isotopes (Piani et al., 2020). Finally, it was also argued that Earth's volatile budget was delivered by a volatile-rich late veneer following termination of accretion and core formation (Wang & Becker, 2013; Fischer-Gödde et al., 2020). Whilst the late veneer is typically estimated to have a mass of about 0.5 % of Earth's mass (M_E) from the abundances of highly siderophile elements (Holzheid et al., 2000, Walker, 2009) much larger masses exceeding 2 % M_E have been suggested based on volatile element systematics (Albarède, 2009; Ballhaus et al., 2013).

Zinc and Cd are chemically similar group 12 elements that primarily occur as divalent cations in natural environments and which are both volatile in a cosmochemical sense. However, whilst Zn is moderately volatile with a 50 % condensation temperature of T_C = 704 K, Cd is a highly volatile element with T_C = 502 K (Wood et al., 2019). Given this, the mantle budgets and stable isotope signatures of the two elements record complementary information on Earth's volatile accretion history. Within Earth's upper mantle, Zn is a lithophile element as mantle sulphides hold less than 1 % of the Zn inventory due to a sulphide-silicate partition coefficient ($D_{Zn}^{sul\text{-}sil}$) of less than about 3 (Li and Audétat, 2012; Kiseeva and Wood, 2013). In fertile spinel lherzolites, mineral Zn concentrations typically decrease in the order spinel ≫ olivine > orthopyroxene > clinopyroxene (Wang et al., 2017). The latter observation is in accord with experimental mineral melt partition coefficients, which indicate that Zn is significantly more compatible in spinel ($D_{Zn}^{sp\text{-}melt}$ = 5.2) than in olivine, orthopyroxene, clinopyroxene and garnet, whereby the latter phases have $D_{Zn}^{min\text{-}melt}$ melt values of about 1, 0.6, 0.4 and 0.2, respectively (Le Roux et al., 2011; Davis et al., 2013). As a consequence, Zn in spinel lherzolites is typically primarily hosted in olivine (>55 %), in intermediate proportions (of about 10–25 %) in orthopyroxene and spinel, with a smaller fraction present in clinopyroxene (<10 %). In accord with the partitioning data, Zn displays mildly incompatible behaviour during mantle melting (Le Roux et al., 2011; Davis et al., 2013; Wang et al., 2017; Sossi et al., 2018).

Even though Cd is regarded as more chalcophile than Zn, it is unlikely that sulphides are a sufficiently important host in the upper mantle to significantly impact Cd behaviour during melting, as previously suggested by Yi et al. (2000). With a $D_{Cd}^{sul\text{-}sil}$ value of about 70 for an upper mantle with 8 % FeO (Kiseeva and Wood, 2013) and 120–250 μg/g S (McDonough and Sun, 1995; Salters and Stracke, 2004), less than 5 % of Cd will be hosted in sulphides, such that essentially lithophile behaviour is also expected for Cd. This conclusion is in accord with the observation of low Cd concentrations in sulphides of basaltic magmas and the finding that the Cd inventory of fertile, sulphide bearing mantle xenoliths is primarily hosted in the constituent silicate minerals rather than in grain boundaries or fluid inclusions (Norman et al., 2004; Witt-Eickschen et al., 2009). Within fertile lherzolites, mineral Cd concentrations decrease in the order clinopyroxene (∼100 μg/g) > orthopyroxene (∼30 μg/g) > olivine (∼15 μg/g). As a consequence, about half of the Cd budget of such rocks is present in clinopyroxene, with the remainder hosted to about equal proportions in orthopyroxene and olivine. In contrast to Zn, spinel is not an important upper mantle host of Cd, due to the low abundance of the mineral and relatively low Cd concentrations of typically less than 50 μg/g (Witt-Eickschen et al., 2009). Published data on the partitioning of Cd during igneous processes are significantly scarcer than for Zn, with experimental mineral-melt partition coefficient available only from a single study and which indicate that Cd is possibly compatible in clinopyroxene and garnet (with $D_{Cd}^{min\text{-}melt} \approx 0.5\text{–}5$) but mildly incompatible ($D_{Cd}^{min\text{-}melt} \approx 0.2\text{–}0.5$) in orthopyroxene and olivine (Adam and Green, 2006). This suggests that Cd should resemble Zn during upper mantle melting, with a mildly incompatible and primarily lithophile behaviour.

Whilst the Zn isotope composition of the bulk silicate Earth (BSE), its reservoirs, and Zn isotope fractionation during common igneous processes have been investigated by several studies (Chen et al., 2013; Doucet et al., 2016; Wang et al., 2017; Sossi et al., 2018; Beunon et al., 2020), very few such data are available for Cd and its isotopes, with no published results for mantle peridotites (Schmitt et al., 2009). This study fills this gap with Cd isotope analyses of a suite of mantle peridotites, mantle melts and other relevant rocks. Most samples were additionally analysed for Zn isotope compositions, to provide context for the Cd isotope data. As such, the current study provides the first comprehensive dataset for mantle rocks to evaluate the Cd isotope composition of the silicate Earth, whilst also enabling a re-evaluation of previous work on the Zn isotope systematics of the BSE. The Cd and Zn results are subsequently employed in the context of available data for chondritic meteorites to improve understanding of terrestrial volatile accretion.

2. Samples

Zinc and Cd isotope analyses were carried out on samples from a variety of tectonic settings and locations to characterise Earth's main silicate reservoirs (Table 1). A total of 14 peridotite samples were analysed, including six spinel lherzolite xenoliths and one harzburgite xenolith from the continental portion of the Cameroon Line volcanic chain of west Africa, which represent melt depletion residues that have undergone variable degrees of metasomatism and partial melt interaction (Lee et al., 1996). Two lherzolites and one harzburgite from the Horoman Peridotite Massif of northern Japan, considered to be a melting residue of a mid-ocean ridge basalt (MORB) source, were also analysed (Takazawa et al., 1996; Yoshikawa and Nakamura, 2000). Isotope data are further presented for four serpentinized abyssal peridotites from Ocean Drilling Program (ODP) Sites

Table 1
Zinc and Cd isotope compositions and concentrations of the samples.

Sample	Location	Lithology	Mass* (g)	δ^{66}Zn (‰)			n#	Zn (μg/g)	δ^{114}Cd (‰)			n#	Cd (ng/g)
Peridotites													
P13	Cameroon Line, Ngaoundéré Plat.	Spinel lherzolite xenolith	2.6	0.22	±	0.04	2	48.7	0.87	±	0.03	2	41.6
P3	Cameroon Line, Ngaoundéré Plat.	Spinel lherzolite xenolith	2.8	0.22	±	0.06	3	43.8	−0.06	±	0.03	2	27.7
C235D	Cameroon Line, Lake Barombi Mbo	Spinel lherzolite xenolith	2.6	0.23	±	0.03	2	51.3	−0.07	±	0.04	2	34.7
C235D	Cameroon Line, Lake Barombi Mbo	Spinel lherzolite xenolith	1.0						−0.16	±	0.12	1	35.7
C235D	Cameroon Line, Lake Barombi Mbo	Spinel lherzolite xenolith	0.8						−0.02	±	0.12	1	35.3
C235D mean									*−0.08*	±	*0.09*		*35.2*
C273Q[$]	Cameroon Line, near Oku	Spinel lherzolite xenolith	3.1	0.25	±	0.04	2	48.9	−0.29	±	0.05	3	42.9
N12[$]	Cameroon Line, Biu Plateau	Harzburgite xenolith	3.0	0.16	±	0.07	2	42.8	−0.08	±	0.05	1	11.5
BZ 134[$]	Horoman Massif, Bozu Section	Spinel lherzolite	3.1	0.22	±	0.05	3	43.9	−0.05	±	0.04	2	15.0
BZ 263[$]	Horoman Massif, Bozu Section	Plagioclase lherzolite	3.1	0.25	±	0.04	3	44.5	0.10	±	0.05	2	25.7
BZ 116[$]	Horoman Massif, Bozu Section	Harzburgite	3.0	0.16	±	0.07	4	40.4	0.10	±	0.04	2	10.8
KH 96-2	Kilbourne Hole, NM, USA	Spinel lherzolite xenolith	0.8						−0.05	±	0.07	1	19.7
920D 11R4 23–27[$]	ODP Hole 920D, MARK Zone	Abyssal harzburgite	3.0	0.12	±	0.06	2	40.2	0.05	±	0.05	2	15.7
920D 22R5 70–74[$]	ODP Hole 920D, MARK Zone	Abyssal harzburgite	3.0	0.13	±	0.06	2	40.0	0.09	±	0.05	2	15.9
895D 8R2 116–118[$]	ODP Hole 895D, Hess Deep	Abyssal dunite	2.1	0.10	±	0.04	4	66.3	−0.02	±	0.05	2	13.5
895E 6R1 51–56[$]	ODP Hole 895E, Hess Deep	Abyssal dunite	3.1	0.11	±	0.06	4	45.7	−0.14	±	0.05	1	6.16
TS-1	Twin Sisters Mt., WA, USA	Dunite	1.0						−0.05	±	0.06	1	5.25
Komatiites													
MT 20	Munro Township, ON, Canada	Komatiite	2.8	0.00	±	0.05	2	62.2	−0.33	±	0.04	3	47.3
M657	Alexo Mine, ON, Canada	Komatiite	1.9	0.14	±	0.05	2	85.2	0.12	±	0.03	2	48.0
KAL-1	Alexo Mine, ON, Canada	Komatiite							−0.12	±	0.10	1	
ZA-1	Belingwe, Zimbabwe	Komatiite	0.5						0.03	±	0.05	2	77.3
Mid-Ocean Ridge Basalts													
POS 221 604 DS-1G	S.Kolbeinsey Ridge	MORB glass	1.0	0.24	±	0.04	3	119	0.06	±	0.05	2	150
POS 221 604 DS-1G	S.Kolbeinsey Ridge	MORB glass	0.5						0.19	±	0.14	2	154
POS 221 604 DS-1G mean									*0.12*	±	*0.09*		*152*
MW 87/2 87-6	East Pacific Rise	MORB glass	1.0	0.28	±	0.06	2	104	0.08	±	0.03	2	158
MW 87/2 87-6	East Pacific Rise	MORB glass	0.5						0.16	±	0.12	2	162
MW 87/2 87-6 mean									*0.12*	±	*0.07*		*160*
A127 DR15	Azores Plateau	MORB glass	0.4	0.23	±	0.06	2	79.6	0.12	±	0.04	1	118
M41/2 130 DS-3	Southern Mid Atlantic Ridge	MORB glass	1.3	0.30	±	0.03	2	43.2	0.02	±	0.04	2	71.4
M41/2 142 DS-2	Southern Mid Atlantic Ridge	MORB glass	1.7	0.29	±	0.04	3	68.5	0.07	±	0.05	2	115
SO80 37 DS-1	Pukao Seamount	MORB glass	1.9	0.44	±	0.03	3	74.1	0.06	±	0.04	2	133
SO80 43 DS-1	Pukao Seamount	MORB glass	1.3	0.27	±	0.05	2	100	0.00	±	0.05	2	132
SO157 54 DS-1	Pacific Antarctic Rise	MORB glass	1.7	0.35	±	0.04	3	96.4	0.08	±	0.05	3	152
SO157 63 DS-1	Pacific Antarctic Rise	MORB glass	2.1	0.33	±	0.02	2	166	0.07	±	0.05	4	302
MD57 D10-1	Indian Ocean	MORB glass	0.2	0.21	±	0.05	3	85.8	0.24	±	0.05	1	132
Ocean Island Basalts													
RE 114	Réunion Island	Basalt	1.6	0.22	±	0.04	4	106	0.48	±	0.06	2	82.9
RE 114	Réunion Island	Basalt	0.5						0.53	±	0.04	1	76.5
RE 114 mean									*0.50*	±	*0.05*		*79.7*
RE 114 olivine	Réunion Island	Olivine from basalt	2.6						0.17	±	0.04	2	22.2
RE 114 olivine	Réunion Island	Olivine from basalt	2.8						0.20	±	0.03	2	22.2
RE 114 olivine mean									*0.18*	±	*0.04*		*22.2*
SNS 24	Budahraun, West Iceland	alkali olivine basalt	1.9	0.32	±	0.02	2	88.6	0.26	±	0.03	2	119
120D	Rurutu Island, Polynesia	Basalt	1.9	0.33	±	0.03	2	152	0.23	±	0.08	5	182
BTHO	Reykjanes Penins., Iceland	Basalt	1.0						0.07	±	0.12	1	92.4
BTHO	Reykjanes Penins., Iceland	Basalt	1.0						−0.04	±	0.12	1	92.9
BTHO mean									*0.01*	±	*0.12*		*92.6*
Loess deposits													
A1530 (L4)	Lingtai, C. Loess Plateau, China	Loess; ~350 ka	1.4	0.18	±	0.03	2	80.3	0.06	±	0.05	4	262
B0020 (L9)	Lingtai, C. Loess Plateau, China	Loess; ~850 ka	0.5						−0.36	±	0.09	1	123
B0020 (L9)	Lingtai, C. Loess Plateau, China	Loess; ~850 ka	0.3						−0.33	±	0.08	2	122
B0020 (L9)	Lingtai, C. Loess Plateau, China	Loess; ~850 ka	0.5						−0.21	±	0.12	1	123

(*continued on next page*)

Table 1 (*continued*)

Sample	Location	Lithology	Mass* (g)	δ^{66}Zn (‰)			n#	Zn (μg/g)	δ^{114}Cd (‰)			n#	Cd (ng/g)
B0020 (L9) mean									*−0.30*	±	*0.10*		*123*
B5366 (L32)	Lingtai, C. Loess Plateau, China	Loess; ~2.5 Ma	1.1	0.24	±	0.03	2	77.3	−0.05	±	0.03	3	94.7
C0950	Jingyuan, W. Loess Plateau, China	Loess	1.1	0.28	±	0.05	3	66.4	0.08	±	0.04	2	137
J1864	Jingyuan, W. Loess Plateau, China	Loess	1.3	0.26	±	0.03	2	59.0	−0.03	±	0.05	4	128
J1865	Jingyuan, W. Loess Plateau, China	Loess	1.3	0.25	±	0.04	2	55.5	0.04	±	0.04	2	115
Do 031.035	Karamaidan, Tajikistan	Loess; ~280 ka	0.8						0.10	±	0.09	1	154
P23.0m	Paks, Hungary	Loess; ~400 ka	1.9	0.26	±	0.03	2	56.3	0.02	±	0.06	5	132
2–8.10	Novaya Etuliya, Moldova	Loess	0.8						0.23	±	0.11	1	197
2–8.20	Novaya Etuliya, Moldova	Loess	1.3	0.21	±	0.06	2	61.3	0.08	±	0.06	2	196
2–8.35	Novaya Etuliya, Moldova	Loess	1.2	0.21	±	0.05	2	59.6	0.06	±	0.04	3	211
Kreuzberg-Bonn	Kreuzberg, Bonn, Germany	Loess	1.3	0.18	±	0.05	2	39.8	0.02	±	0.05	2	114
Basel	Basel, Switzerland	Loess	0.5						0.08	±	0.12	1	148
Geological reference materials													
AGV-2	Guano Valley, OR; USGS	Andesite	1.6	0.28	±	0.03	2	85.1	0.14	±	0.05	3	67.7
JB-2	Oshima Volcano, Japan; GSJ	Island arc basalt	0.5						0.15	±	0.07	1	138
BCR-2	Bridal Veil Flow, OR, USA; USGS	Continental flood basalt	1.0	0.29	±	0.05	5	124	−0.02	±	0.04	1	203
BCR-2	Bridal Veil Flow, OR, USA; USGS	Continental flood basalt	1.0	0.27	±	0.06	4	150	0.03	±	0.04	1	211
BCR-2$	Bridal Veil Flow, OR, USA; USGS	Continental flood basalt	3.0	0.29	±	0.07	1	113	0.02	±	0.05	2	206
BCR-2 mean				*0.28*	±	*0.06*		*129*	*0.01*	±	*0.04*		*207*
BHVO-2	Halemaumau crater, HI; USGS	Basalt (OIB)	1.5	0.33	±	0.05	5	109	0.08	±	0.09	1	90.4
BHVO-2	Halemaumau crater, HI; USGS	Basalt (OIB)	1.5	0.35	±	0.08	2	82.4	0.11	±	0.09	1	86.1
BHVO-2$	Halemaumau crater, HI; USGS	Basalt (OIB)	3.0	0.40	±	0.01	2	89.4	0.08	±	0.05	2	91.3
BHVO-2	Halemaumau crater, HI; USGS	Basalt (OIB)	0.8						0.11	±	0.09	2	86.1
BHVO-2 mean				*0.36*	±	*0.05*		*93.6*	*0.09*	±	*0.08*		*88.5*
BIR-1a	Reykjanes Penins., Iceland; USGS	Dolerite (OIB)	2.7	0.20	±	0.04	2	66.8	0.03	±	0.05	4	93.2

Separate rows for the same sample denote multiple digestions of a sample powder. * mass of individual sample digests. # number of mass spectrometer runs carried out for a given digest; $ samples were digested using a slightly modified procedure (see text for details). Reported uncertainties for sample digests that were analysed only once represent the between-run 2SD precision for replicate runs of the bracketing isotope standard in the same measurement session. For samples that were analysed more than once (using one or several disgests), the uncertainties represent the mean between-run 2SD of individual mass spectrometer runs.

895 (Hess Deep, Eastern Pacific Ocean) and 920 (Mid-Atlantic Ridge Kane, or MARK, Fracture Zone). The MARK zone samples are harzburgites, which are thought to be residues formed by partial melting of fertile upper mantle (Casey, 1997; Niida, 1997), whilst the Hess Deep dunites were likely produced by interaction of refractory harzburgites with basaltic melts (Allan and Dick, 1996; Edwards and Malpas, 1996). Cadmium isotope data were also obtained for one xenolith from Kilbourne Hole, New Mexico (Irving, 1980), and a Twin Sisters dunite (Kruckenberg et al., 2013).

Analyses were carried out on four Archean komatiites, two from Alexo, Canada, and one sample each from Munro Township in Canada and the Belingwe Greenstone Belt in Zimbabwe (Table 1). All four komatiites are spinifex-textured, whereby the Alexo komatiites are derived from the A2 (KAL-1) and A3 (M657) layers of the flow, whilst samples MT 20 and ZA-1 are from the A3 and A2 layers, respectively (Dupré et al., 1984; Arndt, 1986; Jochum et al., 1991; Chauvel et al., 1993; Lahaye and Arndt, 1996; Puchtel and Humayun, 2000). Owing to the high temperatures and associated high degrees of partial melting involved in komatiite formation, they are recorders for the Zn and Cd isotope signature of the Archean mantle, if isotopic effects from crustal contamination, fractional crystallisation and secondary alteration by metamorphism and weathering can be avoided or corrected for (McDonough and Sun, 1995; Dauphas et al., 2010; Sossi et al., 2018).

Also analysed were 10 mid-ocean ridge basalts (MORB) from dredges in the Atlantic, Indian, and Pacific Oceans, six ocean island basalts, from Iceland, Polynesia, Hawaii and Réunion, and olivine separates from the Réunion basalt (Table 1). The Zn and Cd isotope data for these samples reflect the combined effects of partial melting of the mantle, fractional crystallisation, contamination by oceanic crust (for OIB), and possible degassing during subaerial and shallow marine volcanism. Zinc and Cd isotope data are further presented for 13 loess deposits from Asia and Europe to characterise the upper continental crust (Table 1). Loess is suitable for this purpose, owing to the natural mechanical averaging involved in its formation (Taylor et al., 1983; Peucker-Ehrenbrink and Jahn, 2001). For quality control, further Zn and Cd isotope data were acquired for five USGS rock reference materials and these results are included in the characterisation of OIBs (BIR-1a, BHVO-2) and the upper continental crust (AGV-2, BCR-2, JB-2).

3. Analytical techniques

3.1. Laboratories and reagents

Sample preparation for the mass spectrometric analyses was carried out in ISO Class 4 laminar flow hoods within the ISO Class 6 clean room facilities of the MAGIC Laboratories at the Department of Earth Science and Engineering, Imperial College London. All water used was of $\geq$18.2 MΩ cm grade from a Millipore purification system. Distilled 6 M HCl, 12 M HCl, 16 M HNO_3, 28 M HF and 8.5 M HBr as well as double-distilled ethanol (EtOH) were prepared from reagent grade starting materials by sub-boiling distillation in quartz or Teflon stills.

3.2. Sample leaching and digestion

The MORB samples were obtained as chips that were leached before digestion to remove superficial contamination. The chips were first cleaned with water, then EtOH, with agitation in an ultrasonic bath. Samples were then leached at room temperature for 15 min in an ultrasonic bath, first with 0.1 M HCl and then twice with 0.5 M HCl, with water rinsing between each step (Rehkämper et al., 1999b). Sample powders and chips were then weighed before undergoing acid digestion.

Silicate rock samples, weighing between 0.2 and 3.1 g, were first digested on a hotplate in 6–16 mL of a 1 + 2 to 1 + 3 mixture of 16 M HNO_3 and 28 M HF at 80 to 120 °C for 4 to 10 days, and then dried down. The samples were next dissolved in 10–30 mL of a modified aqua regia mixture (1 + 1 of 6 M HCl and 16 M HNO_3) and refluxed at 90 to 130 °C for 5 to 9 days, before being dried and dissolved in 10–30 mL of 6 M HCl and refluxed for 1 to 2 weeks at 100 to 140 °C. Larger acid volumes of up to 60 mL were used for the digestion of the olivine separates. One batch of samples did not undergo a modified aqua regia stage after HF-HNO_3 digestion (see Table 1). Instead, these samples were digested in 10–30 mL of 16 M HNO_3 at 120 °C, and then evaporated, before treatment with 6 M HCl. Spinel phases are known to host Zn in ultramafic rocks (O'Reilly et al., 1991; Wang et al., 2017). Therefore, any remaining mineral residues within the 6 M HCl sample solutions underwent further Parr bomb digestion in 12 M HCl at 130 to 150 °C for 3 to 5 days, before being recombined with the main sample digest.

3.3. Aliquoting and double spiking of samples

Small ($\leq$5%) aliquots of the 6 M HCl sample solutions were utilised for the Zn isotope analyses, with most of the remaining sample solutions used for the Cd isotope measurements. To enable optimal double spiking of the aliquots, the concentrations of Zn and Cd must be known. For samples where the elemental concentrations were not previously determined, appropriate analyses were carried out on a further small (generally $\leq$ 5 %) aliquot. For spiking, the respective sample aliquots were mixed with appropriate volumes of a ^{64}Zn-^{67}Zn double spike with ^{64}Zn/^{67}Zn $\approx$ 2.5 (Arnold et al., 2010) and a ^{111}Cd-^{113}Cd double spike with ^{111}Cd/^{113}Cd $\approx$ 1.7 (Xue et al., 2012). The spiking was dosed to obtain near-optimal molar ratios of spike-derived Zn or Cd to natural Zn or Cd of S/N $\approx$ 1.0 to 1.2, but higher S/N ratios of up to 1.8 were employed for samples where only limited Cd was available for analysis. The spike-sample mixtures were refluxed for 24 h on a hotplate to ensure full equilibration, evaporated to dryness, and dried down twice with a few drops of 6 M HCl.

3.4. Separation of Zn and Cd by anion exchange chromatography

For the separation of Zn, the Zn sample aliquots were taken up in 1 mL of 1 M HCl, refluxed at about 100 °C for 30 min and cooled to room temperature prior to loading onto the previously prepared anion exchange columns. The separation of Zn from the sample matrix employed a single-stage procedure as outlined by Bridgestock et al. (2014) (Table S1, Supplementary Material). This chemical separation produced Zn yields of between about 80 and 100 %, calculated based on the ion beam intensities that were obtained in the isotope analyses. Similarly, the Cd sample aliquots were re-dissolved in 15–30 mL of 3 M HCl prior to loading onto the anion exchange columns. The three-stage Cd column chemistry follows published procedures (Ripperger and Rehkämper, 2007; Xue et al., 2012). After column chemistry, the Cd fractions were extracted twice with heptane, to remove residual organics (Murphy et al., 2016). The Cd yield of the chemical separation was typically between 65 and 100 %, with the exception of five samples, which had yields of about 30 to 50 % (also calculated from the ion beam intensities of the isotope measurements). Most likely, the low yields reflect Cd loss during the chemical separation and purification procedure.

3.5. Zn and Cd stable isotope measurements and data reduction

The Zn and Cd isotope measurements were carried out in the MAGIC Laboratories at Imperial College London. Most analyses were done using a Nu Plasma HR MC-ICP-MS but a Nu Plasma II

instrument was applied for isotopic analysis of Cd-depleted samples where higher sensitivities were desirable. Samples were introduced with a Cetac autosampler and either a Nu instruments DSN-100 or a Cetac Aridus desolvation system using glass nebulizers with nominal uptake rates of 100 µl/min.

The Zn isotope analyses involved monitoring of the ^{64}Zn, ^{66}Zn, ^{67}Zn, and ^{68}Zn ion beams with Faraday collectors equipped with $10^{11}\Omega$ resistors at instrumental sensitivities of > 100 V/(µg/ml). The ion beams at mass numbers 62 ($^{62}Ni^{+}$) and 68.5 ($^{137}Ba^{2+}$) were also measured to correct for isobaric interferences. The presence of Ti was examined, via regular mass scans of sample solutions and the ion beam monitor at mass number 62 (as this also encompasses $^{46}TiO^{+}$). Based on these measurements, the contribution of polyatomic $^{48}TiO^{+}$ to the ion beam at mass number 64 ($^{64}Zn^{+}$) is 5 ppm at most and hence negligible.

The isotopic analyses of samples were carried out relative to bracketing measurements of standard solutions that were prepared as mixtures of the AA-ETH Zn isotope reference material (Archer et al., 2017) with the Zn double spike. All stable Zn isotope compositions were initially determined as $\delta^{66}Zn_{\text{AA-ETH}}$ values relative to the AA-ETH Zn isotope standard:

$$\delta^{66}Zn_{AA-ETH} = \left[\frac{(^{66}Zn/^{64}Zn)_{sample}}{(^{66}Zn/^{64}Zn)_{AA-ETH}} - 1\right] \times 10^{3} \quad (1)$$

In the following, all δ^{66}Zn data are reported relative to the JMC Lyon Zn reference material. To this end, the $\delta^{66}Zn_{\text{AA-ETH}}$ values were converted with the standard conversion identity, which can be approximated as:

$$\delta^{66}Zn = \delta^{66}Zn_{AA-ETH} + \Delta^{66}Zn_{AA-ETH\ -\ JMC\ Lyon} \quad (2)$$

where the isotopic offset between AA-ETH and JMC Lyon Zn, $\Delta^{66}Zn_{\text{AA-ETH - JMC Lyon}}$, is 0.28 ± 0.02 ‰ (Archer et al., 2017). The uncertainty of $\Delta^{66}Zn_{\text{AA-ETH - JMC Lyon}}$ is not propagated in the calculation of δ^{66}Zn because a common offset correction is applied in the community (Archer et al., 2017).

All samples and standards were prepared using 0.1 M HNO_3 to give solutions with S/N ratios and total Zn concentrations (of 50 to 100 ng/ml) that matched to within better than 10 % and 15 % respectively. The isotope measurements were carried out using established protocols (Bridgestock et al., 2014) which feature runs that start with a peak centring routine, three blocks of data acquisition each encompassing 20 five second integration cycles and a preceding 15 s determination of the electronic baselines whilst the ion beam is deflected in the electrostatic analyser. Between runs, the sample introduction system was washed with 0.1 M HNO_3 for 120 s.

The Cd isotope analyses were carried out using established methods (Ripperger and Rehkämper, 2007; Xue et al., 2012) that are similar to those used for Zn. In brief, the ion beams of ^{111}Cd, ^{112}Cd, ^{113}Cd, and ^{114}Cd were monitored for data acquisition, whilst ^{115}In and ^{117}Sn ion beams were measured for interference corrections using Faraday collectors with 10^{11} Ω resistors. Instrumental sensitivity for Cd was typically 200–300 and 600–700 V/(µg/ml) for the Nu Plasma HR-ICP-MS and the Nu Plasma II, respectively. The sample analyses were carried out with Cd solutions of 70 ng/mL (with lower levels employed for a few samples with limited Cd) in 0.1 M HNO_3 relative to matching standards that were prepared as mixtures of NIST SRM 3108 Cd (Abouchami et al., 2013) with the Cd double spike. The Cd stable isotope compositions of the samples are expressed as δ^{114}Cd values relative to the NIST SRM 3108 Cd isotope reference material (Abouchami et al., 2013):

$$\delta^{114}Cd = \left[\frac{(^{114}Cd/^{110}Cd)_{sample}}{(^{114}Cd/^{110}Cd)_{NIST\ SRM\ 3108}} - 1\right] \times 10^{3} \quad (3)$$

Following the mass spectrometric measurements, the reduction of the double spike data was carried out offline using an iterative approach, which corrects for both the monitored isobaric interferences and any laboratory- or instrument-induced mass discrimination (Arnold et al., 2010; Xue et al., 2012). If a sample was only analysed once, the quoted uncertainties of the Zn and Cd isotope data (Table 1) represent the (external or between-run) 2SD precision obtained for multiple analyses of the bracketing isotope standards (AA-ETH Zn or NIST SRM 3108 Cd) in the same measurement session. For samples that were analysed more than once (Table 1), the quoted uncertainties are the average between-run 2SD precision of the individual isotopic runs. The 2SD between-run uncertainties for both repeated sample and standard runs in a measurement session were ±0.01 to ± 0.09 ‰ for δ^{66}Zn, and ±0.02 to ±0.13 ‰ for δ^{114}Cd. These values are similar to the within-run (internal) 2SE uncertainties of individual measurements, which were between ±0.03 and ±0.07 ‰ for δ^{66}Zn, and ±0.03 and ±0.13 ‰ for δ^{114}Cd. In the following, all quoted errors for isotope data represent 2SD uncertainties, unless otherwise stated.

The Zn and Cd concentrations were determined using the isotope dilution technique, which utilised the measured and mass-bias corrected ^{67}Zn/^{68}Zn and ^{111}Cd/^{114}Cd ratios of the spiked sample solutions. Total blanks of the analytical procedures were 0.7 to 1.3 ng for Zn and 0.2 to 20 pg for Cd. Higher blanks of 1.2 to 5.3 ng Zn and of 46 to 123 pg Cd were encountered when Parr bombs were employed in the acid digestion of samples. However, in no case did the blanks reach levels exceeding 1.8 % and 0.3 % of the indigenous Zn and Cd present in samples, respectively, and typical blank contributions were much lower at <0.1 %. The measured concentrations were adjusted for the minor blanks but no blank corrections were applied to the isotopic data, as the Zn and Cd isotope compositions of the blanks were not well-defined and the blank corrections were insignificant given the other analytical uncertainties of the data.

4. Results

4.1. Results for quality control and reference material samples

The secondary London Zn isotope reference material was routinely analysed alongside samples throughout this study, yielding δ^{66}Zn = 0.09 ± 0.05 ‰ (n = 45), consistent with previous measurements (Arnold et al., 2010; Larner and Rehkämper, 2012; Moore et al., 2017). Similarly, repeated analyses of the BAM-I012 Cd isotope reference material yielded a mean of δ^{114}Cd = –1.33 ± 0.07 ‰ (n = 59), in excellent agreement with earlier measurements (Abouchami et al., 2013; Murphy et al., 2016). Furthermore, multiple analyses of the USGS reference materials AGV-2, BCR-2, BHVO-2 and BIR-1a yielded precise Zn and Cd isotope composition and concentration data that are consistently in good agreement with previously published results (Table 1; Tables S3, S4, Supplementary Material). Notably, the Zn and Cd isotope data compiled for BHVO-2 show more scatter than the results obtained for the other rock reference materials, and this may be indicative of minor sample heterogeneity in the BHVO-2 powder.

4.2. Zinc isotope and concentration data

The lherzolites display a narrow range in δ^{66}Zn values, from 0.22 to 0.25 ‰, with Zn concentrations between 44 and 51 µg/g, whilst the harzburgites display an even smaller δ^{66}Zn range from 0.12 to 0.16 ‰, with 40 to 43 µg/g of Zn (Fig. 1a, Table 1). The ODP Hole 895D and 895E Hess Deep dunites are characterised by

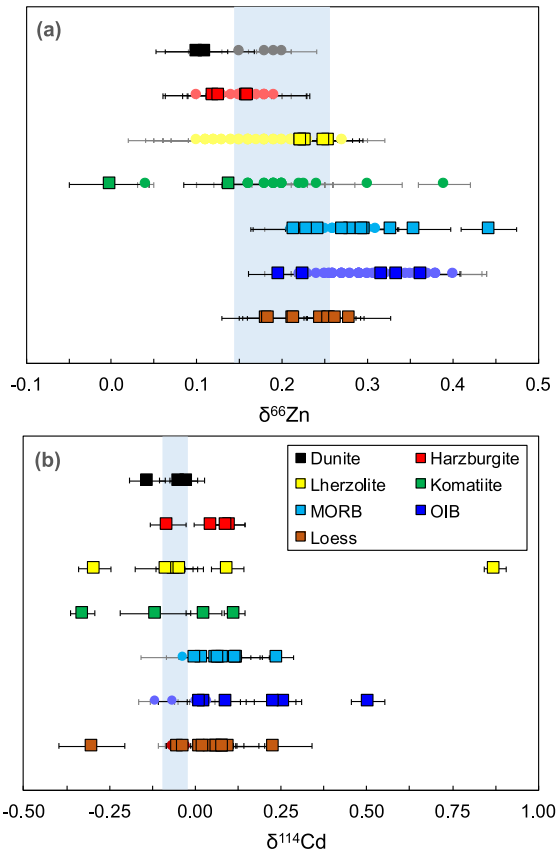

Fig. 1. Stable isotope compositions of (a) Zn and (b) Cd for terrestrial samples from this study (squares) and the literature (circles). The isotope compositions of the BSE with δ^{66}Zn = 0.20 ± 0.05 and δ^{114}Cd = –0.06 ± 0.03 are shown as vertical blue bars. Average Zn isotope compositions are plotted for samples analysed using multiple digestions. Literature data are from Herzog et al. (2009), Mattielli et al. (2012), Chen et al. (2013), Doucet et al. (2016), Wang et al. (2017), Huang et al. (2018a), Huang et al. (2018b), Sossi et al. (2018), Huang et al. (2019), Beunon et al. (2020) for Zn and from Schmitt et al. (2009) for Cd (see Tables S5, S6 of Supplementary Material for details).

Zn contents of 66 and 46 μg/g, respectively, and δ^{66}Zn of 0.10 and 0.11 ‰.

Compared to the peridotites, the mantle melts exhibit more Zn isotope heterogeneity (Fig. 1a, Table 1). The Alexo komatiite M657 (85 μg/g Zn) has a δ^{66}Zn value of 0.14 ± 0.05 ‰, whereas the Munro Township komatiite MT20 (62 μg/g Zn) has δ^{66}Zn = 0.00 ± 0.05 ‰. The MORBs and OIBs also display significant Zn isotope variability, with δ^{66}Zn values of 0.21 to 0.44 ‰ and 0.20 to 0.40 ‰, respectively. Both the MORBs and OIBs are characterised by similar Zn concentrations of 43 to 166 μg/g for the former and 67 to 152 μg/g for the latter. The loess samples, which characterise the continental crust, display δ^{66}Zn values ranging from 0.18 to 0.28 ‰, with Zn concentrations between 40 and 80 μg/g (Fig. 1a, Table 1).

4.3. Cadmium isotope and concentration data

The δ^{114}Cd values of the peridotites, except for Cameroon Line spinel lherzolites P13 and C273Q, fall between –0.16 and 0.10 ‰, with the harzburgites and dunites displaying lower Cd concentrations, of 11 to 16 ng/g and 5 to 14 ng/g, respectively, than the lherzolites, which have 15 to 36 ng/g Cd (Fig. 1b, Table 1). Lherzolite xenoliths P13 and C273Q display more fractionated δ^{114}Cd values of 0.87 ± 0.03 ‰ and –0.29 ± 0.05 ‰, respectively, that are coupled with higher Cd concentrations of about 42 ng/g.

The δ^{114}Cd values of the komatiites vary from –0.33 to 0.12 ‰, with Cd contents of 47 to 77 ng/g. Compared to the komatiites, both MORBs (with 71 to 162 ng/g Cd, except SO157 63 DS-1 with 302 ng/g Cd) and OIBs (76 to 182 ng/g Cd) have higher Cd concentrations. The data acquired for the MORB and OIB samples (except for Réunion basalt RE 114) also display similar δ^{114}Cd ranges, of about 0.00 to 0.24 ‰ and –0.04 to 0.26 ‰, respectively, (Fig. 1b, Table 1). Together, the MORBs and OIBs define an average oceanic basalt δ^{114}Cd of 0.13 ± 0.12 ‰ (n = 21), broadly consistent with previous analyses of basalts (Schmitt et al., 2009; Liu et al., 2019). The Réunion basalt RE 114 is strongly enriched in heavy Cd isotopes relative to the other basalts of this study, with a mean δ^{114}Cd = 0.50 ± 0.05 ‰. In comparison, the RE 114 olivine separate is depleted in Cd relative to the bulk sample (22 ng/g versus 80 ng/g) and features a lower δ^{114}Cd of 0.18 ± 0.04 ‰ (Fig. 1b, Table 1). Most of the loess sediments have δ^{114}Cd values between –0.05 and 0.23 ‰, with the exception of Lingtai sample B0020 (L9), which is characterised by δ^{114}Cd = –0.30 ± 0.10 ‰ (2SD). The Cd concentrations of the loess range from 95 to 262 ng/g.

5. Discussion

5.1. The Zn and Cd isotope composition of the upper continental crust

Previous work has shown that analyses of loess can provide useful constraints on the average elemental and isotope composition of the upper continental crust. Whilst many loess samples reveal signs of chemical weathering it was also shown that even soluble elements, such as Rb and Cs, are typically not depleted in loess due to alteration (Taylor and McLennan, 1985; Gallet et al., 1998; Rudnick and Gao, 2014). Loss of Zn and Cd from loess by weathering is, furthermore, not expected to be associated with severe isotopic effects. In detail, soil formation was found to be associated either with no significant Zn isotope fractionation or, in strongly weathered soils, loss of isotopically heavy Zn (Bigalke et al., 2010; Opfergelt et al., 2017; Little et al., 2019). For Cd, soil profiles revealed preferential removal of isotopically heavy Cd from the soils to fluids (Imseng et al., 2018; Barraza et al., 2019). In the following, the data acquired in this study for European and Asian loess (Fig. 1, Table 1) are evaluated to characterise the Zn and Cd isotope compositions of the upper continental crust.

The loess samples of this study give a mean δ^{66}Zn of 0.23 ± 0.07 ‰ (2SD, n = 9). The observation that the 2SD of the average is only slightly larger than the typical analytical error (of ±0.05 ‰), suggests that isotopic effects from secondary alteration are either absent or minimal. Notably, the loess average overlaps with the δ^{66}Zn data obtained for the igneous crustal rocks AGV-2 (0.28 ± 0.03 ‰) and BCR-2 (0.28 ± 0.06) and is identical, within error, to the published 'lithogenic' Zn isotope value of δ^{66}Zn = 0.27 ± 0.14 ‰, which Little et al. (2016) calculated from data for 50 crustal igneous rocks, sediments and aerosols. The loess data are, furthermore, indistinguishable from a recent lower continental crust δ^{66}Zn estimate of 0.28 ± 0.04 ‰ (95 % SE), as defined by lower crustal xenoliths and granulite terrains from the North China Craton (Zhang et al., 2020). Together, these observations suggest that the Zn isotope composition of the continental crust is relatively homogeneous, on both a global basis and with depth, and similar to that of mantle-derived basalts (Fig. 1).

For Cd, 11 of the 13 analysed loess samples have a limited range of Cd isotope compositions, with δ^{114}Cd of between –0.05 ± 0.03 ‰ and 0.10 ± 0.09 ‰ (Table 1). In contrast, Lingtai loess B0020 (L9) from the Chinese Loess Plateau (CLP) and Moldovian loess sample 2–8.10 are characterized by δ^{114}Cd values of –0.30 ± 0.10 ‰ and 0.23 ± 0.11 ‰, respectively. Notably, some loess sequences from the central CLP experienced particularly extensive pedogenic

processing (Chen et al., 1997; Ding et al., 1999), which may be associated with preferential loss of heavy Cd isotopes (Imseng et al., 2018; Barraza et al., 2019). The origin of the heavy Cd isotope composition of loess 2–8.10 is unclear but could reflect an unusual δ^{114}Cd value for the precursor rocks and/or preferential loss of sulphides enriched in isotopically light Cd. Excluding samples B0020 (L9) and 2–8.10, the Asian and European loess samples define an average δ^{114}Cd = 0.04 ± 0.09 ‰ (2SD, n = 11), in good agreement with three loess analyses of Schmitt et al. (2009). Combining the loess data of this study (Table 1) and Schmitt et al. (2009) gives a mean δ^{114}Cd of 0.03 ± 0.10 ‰ (2SD, n = 14) for the upper continental crust, in excellent agreement with a previous upper continental crust estimate of 0.05 ± 0.10 ‰ that was based on continental sulphides (Schmitt et al., 2009; Rehkämper et al., 2011).

5.2. Zinc isotopes in the mantle and mantle-derived rocks

5.2.1. The Zn isotope compositions of peridotites

The lherzolites from the Cameroon Line and the Horoman peridotite massif define a mean δ^{66}Zn of 0.23 ± 0.03 ‰ (2SD, n = 6) and the data resemble results obtained for lherzolites from the North China Craton (Wang et al., 2017) and the Italian Alps (Huang et al., 2018a) (Fig. 1a, Tables 1, 2). In comparison, slightly lighter Zn isotope compositions were determined for lherzolites from the Balmuccia lherzolite massif (Sossi et al., 2018). The lherzolites analysed here have Zn concentrations of about 44 to 51 μg/g and are thus slightly depleted in Zn relative to BSE estimates of about 54 μg/g Zn (McDonough and Sun, 1995; Wang et al., 2018), likely attesting to minor melt depletion during their formation (Lee et al., 1996; Takazawa et al., 1996; Yoshikawa and Nakamura, 2000). Previous studies furthermore indicate that Cameroon Line and Horoman peridotites were subject to variable, but generally light to moderate, metasomatism (Takazawa et al., 1992; Lee et al., 1996; Takazawa et al., 1996; Anguelova et al., 2022), and in the case of the latter, re-enrichment by sulphides (Rehkämper et al., 1999a). The limited variability of our lherzolite Zn isotope compositions and the lack of significant Zn isotope effects relative to many previously analysed lherzolites suggests that such processes, as well as surficial weathering, had little impact on the δ^{66}Zn values of the Cameroon Line and Horoman samples.

Compared to the lherzolites, the harzburgites from the Cameroon Line (N12) and Horoman (BZ 116) as well as the MARK Zone abyssal harzburgites are more depleted in Zn, with concentrations of 40 to 43 μg/g, and they display lower δ^{66}Zn values of between 0.12 ± 0.06 ‰ and 0.16 ± 0.07 ‰ (Table 1). Similar results were obtained for other previously analysed harzburgites (Doucet et al., 2016; Wang et al., 2017) and possibly reflect extraction of an isotopically heavy melt. The Hess Deep dunites also display light Zn isotope compositions, but these samples are not true melt depletion residues, instead forming from the interaction of basaltic melts with refractory harzburgites (Allan and Dick, 1996; Edwards and Malpas, 1996). Notably, the dunites and harzburgites together define a mean δ^{66}Zn = 0.13 ± 0.05 ‰ (2SD, n = 6) that is significantly lower compared to the lherzolite average.

Table 2
Mean Zn isotope compositions of mantle peridotites from different localities and the BSE estimate of this study.

Locality	δ^{66}Zn	2SD	Reference
Vitim and Tariat lherzolites	0.30	0.03	Doucet et al. (2016)
Ivrea-Verbano Zone	0.17	0.09	Sossi et al. (2018); Huang et al. (2018a)
North China Craton	0.19	0.06	Wang et al. (2017)
Bohemian Massif (Horni Bory)	0.20	0.05	Huang et al. (2019)
Baffin Island (picrite mantle)	0.20	0.03	McCoy-West et al. (2018)
Cameroon Line	0.23	0.03	This study
Horoman Peridotite	0.23	0.04	This study
Bulk Silicate Earth δ^{66}Zn	***0.20***	***0.05***	**This study (without Doucet et al. 2016 data)**
Bulk Silicate Earth δ^{66}Zn	*0.22*	*0.08*	This study (all data)

Shown for the Ivrea-Verbano Zone and North China Craton are mean values and 2SD of lherzolite data for these localities. Bohemian Massif value represents mean of two analyses, with 2SD representing average measurement uncertainty. Baffin Island value represents the calculated Zn isotope composition of the picrite mantle source. The Cameroon Line and Horoman Massif mean values are based on the peridotite data of this study (see text).

5.2.2. The Zn isotope compositions of komatiites

Komatiites form by extensive partial melting of the mantle at high temperatures and often record only minor fractional crystallisation and contamination by continental crust. As such, they are, in principle, suitable archives to determine the isotope compositions of Zn and other elements in the Archean mantle (McDonough and Sun, 1995; Dauphas et al., 2010; Sossi et al., 2018). The two komatiites analysed here have different δ^{66}Zn values, with results of 0.14 ± 0.05 ‰ for M657 from Alexo and 0.00 ± 0.05 ‰ for MT20 from Munro Township (Fig. 1, Table 1). The origin of this isotopic difference is uncertain because both samples are derived from the spinifex-textured A3 zones of their flows and both have similar Zn/Fe ratios (of ~9), which are indicative of limited Zn loss or addition by secondary alteration (Sossi et al, 2018). Notably, the Alexo komatiite of this study and 12 of 13 spinifex and olivine cumulate komatiites analysed by Sossi et al.(2018) from six different localities have δ^{66}Zn values of between 0.14 and 0.20 ‰ (Fig. 1a, Table S5). This suggests that these samples most likely record a relatively homogeneous Archean mantle composition, with a mean of 0.18 ± 0.04 ‰ (2SD, n = 13). In contrast, a Barberton olivine cumulate komatiite of Sossi et al (2018) and sample MT 20, which was sampled from the lower (A3) part of the spinifex zone and features relatively high MgO and Ni concentrations coupled with low Cr, have much lower δ^{66}Zn values of or close to 0 ‰. Whilst it is conceivable the light Zn isotope signatures of the latter two komatiites reflect accumulation of olivine characterised by low δ^{66}Zn, such an origin is not readily reconciled with the limited Zn isotope fractionation that was inferred for magmatic systems (Sossi et al., 2018).

5.2.3. The Zn isotope compositions of oceanic basalts

Extending from the peridotites, the komatiites and oceanic basalts define an igneous 'mantle array' in a plot of δ^{66}Zn versus Zn concentration, whereby the melts feature higher Zn abundances coupled with slightly heavier Zn isotope compositions (Fig. 2a, b). The MORB and OIB samples display similar Zn isotope compositions, with a combined average δ^{66}Zn of 0.30 ± 0.14 ‰ (2SD, n = 17), generally consistent with previously analysed basalts (Herzog et al., 2009; Chen et al., 2013; Wang et al., 2017; Huang et al., 2018b; Beunon et al., 2020). The observed variability of basalt compositions clearly exceeds the analytical uncertainty (of about ±0.05 ‰; Table 1), presumably reflecting Zn isotope variations from both primary igneous and subsequent secondary processes.

The higher δ^{66}Zn values and Zn concentrations of mantle melts relative to lherzolites is mirrored by the lower δ^{66}Zn values and Zn concentrations of refractory harzburgites and dunites. These systematic differences most likely reflect, to a first order, isotope fractionation and incompatible behaviour of Zn during partial melting of the mantle and melt differentiation. During melting, isotopically heavy Zn preferentially partitions into the melt phase, leaving behind a more refractory and isotopically light peridotite residue that is depleted in Zn (Fig. 2a, b). Previous studies have come to similar conclusions (Doucet et al., 2016; Wang et al., 2017; Sossi et al., 2018), but the driver for isotope fractionation during partial melting remains a topic of debate. Wang et al. (2017) measured

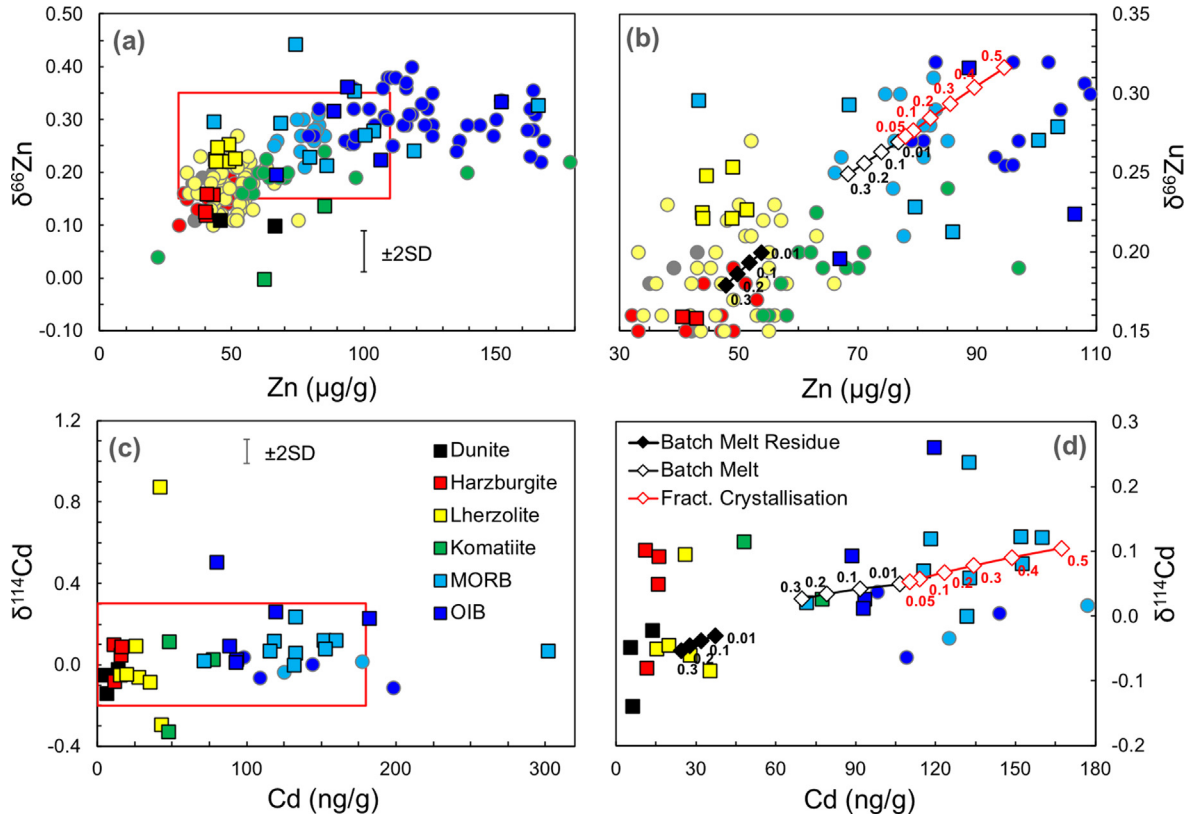

Fig. 2. Plots of (a), (b) δ^{66}Zn versus Zn concentrations and (c), (d) δ^{114}Cd versus Cd concentrations for peridotites and mantle melts. The red boxes in panels (a) and (c) show the areas highlighted in panels (b) and (d). Squares are data from this study and smaller circles represent literature values (see Fig. 1. and Tables S5, S6 of Supplementary Material for data sources). The results of batch melting and fractional crystallisation calculations (see Text in Supplementary Material) are superimposed on the igneous data in panels (b) and (d). Open and solid black diamonds represent the melts and residual peridotites formed after 1 to 30 % batch mantle melting. Open red diamonds show the melt compositions after 5 to 50 % fractional crystallisation of a melt that was obtained at F = 1 %. In panel (b) the initial δ^{66}Zn and Zn concentration are 0.20 ‰ and 54 µg/g, respectively; values of D_{Zn} = 0.7 and $\Delta^{66}Zn_{mantle\text{-}melt}$ = −0.07 ‰ were used in the calculations (see text for details). In panel (d) the initial δ^{114}Cd and Cd concentration are −0.06 ‰ and 38 ng/g, respectively; values of D_{Cd} = 0.35 and $\Delta^{114}Cd_{mantle\text{-}melt}$ = −0.09 ‰ were used in the calculations (see text for details).

elevated δ^{66}Zn in spinel separates from multiple peridotites but found no significant differences in the δ^{66}Zn values of olivine, clinopyroxene and orthopyroxene or any significant correlation between peridotite δ^{66}Zn and extracted melt fraction or pressure of equilibration. Based on non-modal fractional melting models, Wang et al. (2017) showed that the observed isotope fractionations could result from consumption of isotopically heavy spinel during the melting process. Sossi et al. (2018) argued, however, that spinel abundances in lherzolites are too low to act as a significant control on peridotite δ^{66}Zn. In contrast, they suggested that Zn isotope fractionation is controlled by differences in the coordination number of Zn in olivine (octahedral coordination) and melt (tetrahedral coordination), whereby the latter is enriched in isotopically heavy Zn due to the stronger Zn–O bonding.

Fig. 2a confirms that Zn is incompatible during mantle melting. This is in accord with previous studies, which inferred bulk solid–liquid distribution coefficients, D_{Zn}, of between about 0.6 and 1.0 for the partitioning of Zn during melting of peridotites (Le Roux et al., 2011; Davis et al., 2013; Wang et al., 2017; Sossi et al., 2018; Beunon et al., 2020). Based on the inter-mineral fractionations observed by Wang et al. (2017), Sossi et al. (2018) inferred a mantle–melt Zn isotope fractionation of $\Delta^{66}Zn_{mantle\text{-}melt}$ = −0.07 ‰ , whilst Chen et al. (2013) concluded that Zn isotope fractionation during high-temperature magmatic differentiation is unlikely to exceed ± 0.10 ‰, based on analyses of volcanic rocks from Kilauea Iki lava lake and Hekla volcano. Notably, similar estimates of D_{Zn} = 0.75 and $\Delta^{66}Zn_{mantle\text{–}melt}$ = −0.03 ± 0.09 ‰. were obtained in this study, based on the assumption that the partitioning of Zn between mantle and continental crust is governed by magmatic processes (Hofmann, 2014; see Supplementary Materials).

The results of simple, illustrative batch melting and (subsequent) fractional crystallisation calculations (see Supplementary Materials) are superimposed onto the global peridotite and mantle melt data of Fig. 2b. The modelling assumes an initial mantle source with 54 µg/g Zn (McDonough and Sun, 1995; Wang et al., 2018) and δ^{66}Zn = 0.20 ‰ and employs parameters of D_{Zn} = 0.7 and $\Delta^{66}Zn_{mantle\text{-}melt}$ = −0.07 ‰, in accord with available constraints. Notably, the calculated igneous trends demonstrate that, to a first order, the variable Zn isotope compositions and concentrations of the global mantle array seen in Fig. 2a, b can be explained by partitioning of mildly incompatible Zn into the melt phase during igneous processes and associated enrichment of isotopically light Zn in the melt.

The significant scatter of data within and about the trend of Fig. 2a, b is readily explained by additional primary and secondary processes. The variable Zn concentrations and isotope compositions exhibited by OIBs may reflect melting of more fertile mantle reservoirs that were enriched by admixing of eclogitic oceanic crust (Beunon et al., 2020) or possibly fluids expelled from dehydrating ocean crust in subduction zone settings. Similarly, mantle heterogeneities associated with contamination by subducted carbonate sediments can cause large shifts in the Zn isotope compositions of mantle melts (Liu et al., 2016; Liao et al., 2020), whilst some degree of Zn isotope heterogeneity may also have developed in the mantle by millions of years of melt depletion (Wang et al., 2017; Zhu et al., 2021). Depth dependant changes in mineralogy

may further impact D_{Zn} and $\Delta^{66}Zn_{mantle\text{-}melt}$ values, causing further scatter in Fig. 2a, b. In particular, previous studies hint at a possible decrease in the D_{Zn} of olivine, pyroxenes, and garnet, and an increase for spinel, at higher temperatures (Horn et al., 1994; Adam and Green, 2006; Le Roux et al., 2011; Davis et al., 2013). Secondary processes, including fluid exsolution, serpentinization, as well as metasomatism and melt percolation with associated Zn transfer (Telus et al., 2012; Wang et al., 2017; Huang et al., 2018a; Huang et al., 2019) can also generate Zn isotope fractionations that may be equal to or greater than those resulting from magmatic processes. Notably, despite these many potential avenues for generating Zn isotope variability, the generated variations are relatively small such that the igneous array remains fairly well defined.

5.2.4. The Zn isotope composition of the bulk silicate Earth

The average $\delta^{66}Zn$ values of the Horoman and Cameroon Line lherzolites and results for previously studied lherzolite localities are combined in the following to obtain a new estimate for the $\delta^{66}Zn$ of the BSE (Table 2). This estimate does not include results for harzburgites and dunites, as their $\delta^{66}Zn$ values may be impacted by melt depletion even though current melting models do not predict significant Zn isotope fractionation in peridotite residues for up to 30 % melt extraction (Sossi et al., 2018). Our preferred $\delta^{66}Zn_{BSE}$ estimate is obtained by averaging the mean Zn isotope data determined for lherzolites from five distinct localities, with each characterised by at least two samples. In addition, the compilation includes the $\delta^{66}Zn$ value of 0.20 ± 0.03 ‰ determined for the Baffin Island parental mantle reservoir by McCoy-West et al. (2018). However, the fertile Vitim and Tariat off-craton lherzolites of Doucet et al. (2016) are excluded from our preferred $\delta^{66}Zn_{BSE}$ estimate, as these rocks display unusually high $\delta^{66}Zn$ values of about 0.3 ‰ and the origin of this heavy Zn isotope signature is unclear. Together, the selected localities define a $\delta^{66}Zn_{BSE}$ of 0.20 ± 0.05 ‰ (2SD; Table 2), consistent with previous BSE estimates (Wang et al., 2017; Sossi et al., 2018). However, inclusion of the Doucet et al. (2016) data produces only a marginally higher $\delta^{66}Zn_{BSE}$ value of 0.22 ± 0.08 ‰ (2SD; Table 2).

Notably, our new $\delta^{66}Zn_{BSE}$ value overlaps with the mean $\delta^{66}Zn$ = 0.18 ± 0.04 ‰ (2SD, n = 13) determined for komatiites. This latter average, which is based on the data for spinifex-textured and olivine cumulate komatiites of Sossi et al. (2018) and the Alexo komatiite M657 of this study, should approximate the Zn isotope composition of the Archean mantle. The close overlap of the komatiite mean with the peridotite-based $\delta^{66}Zn_{BSE}$ estimate suggests that the Zn isotope composition of the mantle remained relatively constant since the Archean, as previously inferred by Sossi et al. (2018).

5.3. Cadmium isotopes in the mantle and mantle-derived melts

5.3.1. The Cd isotope compositions of peridotites

The Cd isotope compositions of the peridotites are more variable than those of Zn, both overall and for individual localities (Fig. 1a, b, Table 1). In particular, the Cameroon Line spinel lherzolites P13 and C273Q exhibit strongly fractionated Cd isotope compositions of 0.87 ± 0.03 ‰ and −0.29 ± 0.05 ‰, respectively. In contrast, the remaining spinel lherzolites from the Cameroon Line, the Horoman Massif and Kilbourne Hole (termed 'undisturbed' in the following) display a narrow range of $\delta^{114}Cd$ values with a mean of −0.06 ± 0.03 ‰ (2SD, n = 4), whereas the Horoman plagioclase lherzolite has a much higher $\delta^{114}Cd$ of 0.10 ± 0.05 ‰. Furthermore, a single harzburgite has a $\delta^{114}Cd$, of −0.08 ± 0.05 ‰, which resembles the undisturbed spinel lherzolites, whereas three others have significantly heavier isotope compositions, with $\delta^{114}Cd$ values of between 0.05 ± 0.05 ‰ and 0.10 ± 0.04 ‰. Finally, the three dunites from the Hess Deep and Twin Sisters have negative $\delta^{114}Cd$ values of −0.14 ± 0.05 ‰ to −0.02 ± 0.05 ‰, similar to the spinel lherzolites (Fig. 1, Table 1).

Whilst the variable $\delta^{114}Cd$ values observed for peridotites are difficult to understand in detail, the Cd concentrations show more straightforward systematics. In particular, the lherzolite Cd concentrations are on average (31 ± 10 ng/g; 1SD, n = 9) about 3x higher than those of the harzburgites and dunites (11 ± 4 ng/g; 1SD, n = 7), and slightly lower than, but still within uncertainty of, previous BSE estimates of about 38 ng/g (McDonough and Sun, 1995; Witt-Eickschen et al., 2009; Wang et al., 2018). This difference is, at least in part, most likely a consequence of melt extraction with associated depletion of Cd in the residue. Given that oceanic basalts have Cd isotope compositions that are typically either similar to or heavier compared to the 'undisturbed' spinel lherzolites of this study, melt extraction should produce mantle residues with $\delta^{114}Cd$ values that are similar to or lower than those of the lherzolites. In contrast, three of the four analysed harzburgites have much heavier Cd isotope compositions, which must therefore be of secondary origin (Figs. 1, 2c, d).

The Cd isotope systematics of many, if not most, peridotites studied here are hence most likely a consequence of melt extraction, with either limited or no resolvable isotope fractionation in the residue, and subsequent overprinting by one or several secondary processes. Notably, there is no clear correlation between changes in Cd isotope compositions and petrographic indicators of metasomatism and melt-rock reaction. For example, the two strongly fractionated Cameroon Line samples C273Q and P13 have the highest Cd concentrations of the peridotites analysed here, and this may indicate that the unusual Cd isotope signatures are a consequence of secondary processes that enriched the Cd abundances of the rocks. However, both samples show less petrographic and geochemical evidence of secondary alteration than peridotite P3 (Lee et al., 1996), which appears to have an unperturbed Cd isotope composition. Furthermore, samples from both the Hess Deep and MARK ODP sites were affected by melt depletion and multiple secondary processes, including melt percolation and reaction and serpentinization (Allan and Dick, 1996; Edwards and Malpas, 1996; Casey, 1997; Niida, 1997; Rehkämper et al., 1999a). Whilst the Hess Deep dunites display Cd isotope compositions generally in line with most of the Cameroon Line peridotites, the MARK harzburgites display heavy Cd isotope enrichments. This may imply that some combination of the aforementioned processes can lead to enrichments of heavy Cd isotopes in residual mantle rocks.

Of further interest is the previous conclusion that the Zn isotope compositions that were determined for a subset of the peridotites primarily record igneous processes, with little or no significant isotope effects from subsequent secondary processes and weathering. As the Cd isotope compositions of peridotites appear to be more susceptible to alteration, this indicates that secondary reactions more readily affect the ng/g-level abundances of Cd than the μg/g concentrations of Zn. Such an explanation is viable if alteration impacts minor phases that are important hosts for Cd but not Zn or involves reactions with fluids or melts that have high Cd/Zn ratios. Notably, Zn is primarily hosted in olivine, volumetrically the most abundant mineral in peridotites, whilst Cd is concentrated in clinopyroxene, which is typically a modally minor phase. Cadmium is, furthermore, more volatile in high temperature environments than Zn (Hinkley et al., 1994; Rubin, 1997), and such mobility may also generate stable isotope effects for Cd in peridotites.

5.3.2. The Cd isotope compositions of komatiites

The four analysed komatiites show significant Cd isotope variability, whereby Munro Township sample MT 20 has an unusually

low δ^{114}Cd of –0.33 ± 0.04 ‰ relative to the other rocks (Table 1). Notably, MT20 also has an atypically light Zn isotope composition that diverges from published Zn isotope data for other komatiites from Munro and other localities (Fig. 1; Table S5). Whilst the unusual Zn isotope signature of this sample may have an igneous origin, it is unclear whether this can account for the light Cd isotope composition, for example by accumulation of olivine or possibly sulphides with low δ^{114}Cd. Given that the Cd isotope compositions of two peridotites were altered by >0.25 ‰ by secondary processes to both higher and lower δ^{114}Cd values, such an origin is also probable in this case. Weathering processes alone are an unlikely cause, however, as even strongly weathered soils typically show Cd isotope shifts of less than 0.3 ‰ (Imseng et al., 2018; Barraza et al., 2019).

The δ^{114}Cd values of the three remaining spinifex-textured komatiites from Alexo and Belingwe range from –0.12 ± 0.03 ‰ to 0.12 ± 0.03 ‰ (Table 1, Fig. 1b). With an isotopic variability that exceeds the analytical uncertainty by about a factor of x2 to x3, the Cd isotope compositions of these samples were likely also affected by secondary alteration. Despite this, the mean δ^{114}Cd value defined by the komatiites, of 0.01 ± 0.19 ‰ (2SD, n = 3), overlaps with the Cd isotope compositions of the 'undisturbed' spinel lherzolites (Fig. 1b). Notably, sample ZA-1, which is derived from the particularly fresh Belingwe komatiite flow (Nisbet et al., 1987; Chauvel et al., 1993), is characterised by an intermediate δ^{114}Cd value of 0.03 ± 0.05 ‰.

5.3.3. The Cd isotope composition of oceanic basalts

Similar to Zn, the Cd data of mantle melts define an igneous array that extends from the peridotites in a diagram of δ^{114}Cd versus Cd concentration (Fig. 2c, d). As for Zn, the Cd concentrations also increase from the peridotites through the komatiites to the oceanic basalts, most likely as a consequence of incompatible behaviour of Cd (Yi et al., 2000; Witt-Eickschen et al., 2009). However, the isotopic effects are less clearly defined than for Zn (Fig. 2a, b), which at least in part reflects the greater degree of scatter in the Cd isotope data, particularly for the peridotites and komatiites. In detail, the MORB and OIB samples show a mean δ^{114}Cd of 0.13 ± 0.12 ‰ (2SD, n = 16) that is slightly enriched in heavy Cd isotopes relative to the peridotites. This marginal enrichment and the isotopic variability, which clearly exceeds the analytical errors, further argue for some degree of Cd isotope fractionation during partial melting of the mantle and melt differentiation. Given that the Zn and Cd data of Fig. 2a, b and c, d, respectively, define similar trends, it is reasonable to conclude that the Cd mantle array of Fig. 2c, d is also primarily the result of incompatible behaviour and associated isotope fractionation of Cd during partial melting and fractional crystallisation.

Published constraints on the partitioning and isotope fractionation of Cd during igneous processes are significantly scarcer than for Zn. Based on analyses of MORB and OIB, Yi et al. (2000) inferred that Cd is moderately or slightly incompatible during mantle melting with a bulk mineral-melt D_{Cd} of > 0.01. The only experimental partitioning data available constrain the distribution of Cd between mica- and amphibole-bearing garnet lherzolite and hydrous basanitic melt (Adam and Green, 2006). For clinopyroxene, garnet, orthopyroxene and spinel, the latter study determined mineral melt partition coefficients of $D_{Cd}^{cpx\text{-}melt}$ = 0.5–2.5 (n = 8), $D_{Cd}^{grt\text{-}melt}$ = 2.2–4.7 (n = 2), $D_{Cd}^{opx\text{-}melt}$ = 0.5 (n = 1) and $D_{Cd}^{ol\text{-}melt}$ = 0.17–0.22 (n = 2). These affinities are roughly in accord with the inter-mineral distribution coefficients of $D_{Cd}^{cpx\text{-}ol} \approx 5.2$ and $D_{Cd}^{opx\text{-}ol} \approx 2.2$ that were inferred from in-situ mineral analyses of spinel lherzolites (Witt-Eickschen et al., 2009). Using $D_{Cd}^{ol\text{-}melt}$ = 0.2, $D_{Cd}^{opx\text{-}melt}$ = 0.45 and $D_{Cd}^{cpx\text{-}melt}$ = 1, these results yield a bulk D_{Cd} = 0.41 for a typical spinel lherzolite (0.54 ol, 0.26 opx, 0.18 cpx, 0.02 sp), with the reasonable assumption that spinel has no bearing on the partitioning of Cd (Witt-Eickschen et al., 2009). Notably, a similar D_{Cd} value of about 0.48 can be inferred for mantle melting from the Cd concentration ratio of the BSE versus the continental crust (Hofmann, 2014; see Supplementary Materials for details). Furthermore, Fig. 3a shows that the BSE-normalised concentrations of Cd and Zn are positively correlated across mantle melts and peridotites, indicating that the two elements behave similarly during igneous processes. The more rapid increase of Cd versus Zn concentrations in mantle melts (with a slope of about 2) thereby suggests that the former element is more incompatible than the latter, with $D_{Cd}/D_{Zn} \approx 0.5$. Assuming D_{Zn} = 0.7 (Sossi et al., 2018; Beunon et al., 2020) this yields D_{Cd} = 0.35, in accord with our estimate derived from mineral-melt D values.

As of yet, there are no published constraints on Cd isotope fractionation during partial melting of the mantle and subsequent melt differentiation. Fig. 3b shows that whilst there is a small but well-resolved difference in δ^{66}Zn between peridotites and mantle melts, such a difference is not clearly resolved for Cd isotopes. Using the inferred compositions of the continental crust (δ^{114}Cd = 0.03 ± 0.10 ‰) and the BSE (δ^{114}Cd = –0.06 ± 0.03 ‰; see below), a $\Delta^{114}Cd_{mantle\text{-}melt}$ of –0.09 ± 0.10 ‰ can be estimated for partial melting of the mantle, in accord with the previous conclusion that isotope fractionation during igneous processes generates either a small or negligible enrichment of heavy Cd isotopes in mantle melts (Hofmann, 2014; see Supplementary Materials for details). Unfortunately, the large range of δ^{114}Cd values exhibited by peridotites and basalts limits any further inferences about the extent and origin of Cd isotope fractionation during igneous processes.

Importantly, the results of the batch melting and fractional crystallisation calculations confirm that the global Cd isotope systematics observed for peridotites and mantle basalts most likely

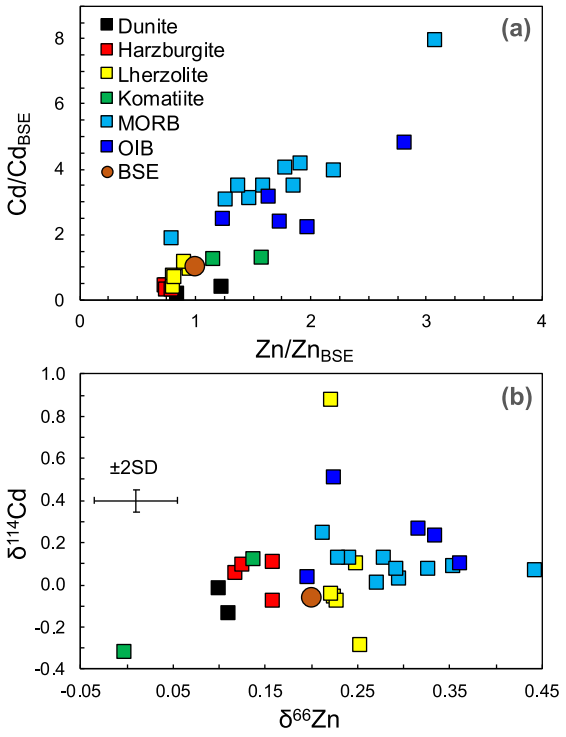

Fig. 3. Plots of (a) BSE-normalised Cd versus BSE-normalized Zn concentrations and (b) δ^{114}Cd versus δ^{66}Zn for the peridotites, komatiites and oceanic basalts analysed in this study. The BSE composition, with 54 µg/g Zn, δ^{66}Zn = 0.20 ± 0.05 ‰ and 38 ng/g Cd, δ^{114}Cd = –0.06 ± 0.03 ‰, is also shown in both panels (see text for details).

primarily reflect melting and melt differentiation of mantle material. The modelling presented in Fig. 2c, d uses a mantle source composition with 38n/g Cd and δ^{114}Cd = –0.06 and employs reasonable parameters of D_{Cd} = 0.35, such that Cd is marginally more incompatible than Zn, and $\Delta^{114}Cd_{mantle\text{-}melt}$ of –0.09 ‰. It is noted, however, that the modelling results of Fig. 2 are only presented for illustration, particularly because the simple calculations do not consider differences in melt source compositions and the dynamics of partial melting and melt differentiation, all factors that will invariably generate significant scatter about and beyond the petrogenic trends shown in Fig. 2.

Additional scatter is furthermore expected for the Cd data of mantle melts as a result of secondary processes, particularly given the significantly lower Cd concentration of igneous rocks compared to Zn. Of particular relevance is magmatic outgassing of volatile Cd and associated isotope fractionation in oceanic basalts. Prytulak et al. (2013) found a Mariana arc lava that was anomalously enriched in heavy Tl isotopes, which they attributed to volcanic degassing. A number of studies have furthermore shown that Cd is amongst the elements that are most efficiently lost from silicate melts during magmatic outgassing and most strongly enriched in volcanic gases (Hinkley et al., 1994; Rubin; 1997; MacKenzie and Canil, 2008; Norris and Wood, 2017; Sossi et al., 2019; Zelenski et al., 2021). Such outgassing and associated isotope fractionation may hence be responsible for the unusually high δ^{114}Cd value of Réunion Island basalt RE 114 (Table 1). Notably, the large Cd isotope difference of >0.3 ‰ between the RE 114 whole rock (δ^{114}Cd = 0.50 ± 0.05 ‰) and olivine phenocrysts from this sample (δ^{114}Cd = 0.18 ± 0.04 ‰) is unlikely to record equilibrium isotope fractionation during differentiation, given the limited extent of Cd isotope fractionation that was inferred for igneous processes (with $\Delta^{114}Cd_{mantle\text{-}melt}$ < 0.2 ‰). Rather, the heavy Cd isotope composition of RE 114 is most likely due to loss of volatile Cd and with preferential loss of light Cd isotopes during open system degassing of the magma. In contrast, the lighter Cd isotope composition of the RE 114 olivine separate reflects olivine fractionation prior to Cd degassing and associated isotope fractionation. The RE 114 olivine is also depleted in Cd relative to the whole rock (22 versus 80 ng/g), confirming that Cd is moderately incompatible in olivine relative to melt.

5.3.4. The Cd isotope composition of the bulk silicate Earth

The data obtained for peridotites and mantle melts indicate that igneous processes generate at most minor Cd isotope fractionations. As such, a straightforward estimate for the δ^{114}Cd value of the BSE can be determined from the overall mean determined for all peridotites, including the harzburgites and dunites, but excluding the most anomalous samples C273Q and P13. This approach gives a $\delta^{114}Cd_{BSE}$ of –0.02 ± 0.15 ‰ (2SD, n = 12), A more precise and robust BSE estimate can be obtained, however, from the results obtained for four 'undisturbed' spinel lherzolites from three localities, which define a mean $\delta^{114}Cd_{BSE}$ value of –0.06 ± 0.03 ‰ (2SD). This $\delta^{114}Cd_{BSE}$ estimate is preferred because it is based on data that was at most marginally effected by Cd mobilisation and isotope fractionation during secondary alteration of the rocks.

Our result is in good agreement with a previous BSE estimate of –0.03 ± 0.10 ‰ (Schmitt et al., 2009; Rehkämper et al., 2011) but is more robust because it does not rely on data for oceanic basalts or samples from the continental crust, which may be biased by any isotope fractionation that occurs during partial melting and melt differentiation. Notably, our $\delta^{114}Cd_{BSE}$ estimate is also within error of the komatiite δ^{114}Cd mean of 0.01 ± 0.19 ‰ (2SD, n = 3), which excludes anomalous sample MT20. Assuming that the komatiite average is representative of the Archean mantle, this would indicate that the Cd isotope composition of the silicate Earth remained nearly constant through time. However, the komatiite mean has a large error, such that the conclusion is subject to significant uncertainty.

5.4. Zinc and Cd stable isotopes in comparison to chondritic meteorites

Whilst there is considerable debate about the timing and nature of Earth's volatile delivery, the majority of investigations concur that volatile species were most likely added in the later stages of accretion by material that was akin in composition to carbonaceous or enstatite chondrites or a mixture of both (Albarède, 2009; Wood et al., 2010; Fischer-Gödde et al, 2020). To further assess the provenance of terrestrial volatiles, it is of interest to compare the BSE Zn and Cd isotope compositions with data for chondritic meteorites from published investigations (Fig. 4). In a plot of δ^{66}Zn versus Zn concentrations, the majority of carbonaceous chondrites define a clear trend that extends from volatile rich CI chondrites with $\delta^{66}Zn \approx 0.45$ ‰, through CM and CV to more volatile depleted CO and CR chondrites with lower δ^{66}Zn (Fig. 4a). Although many enstatite and ordinary chondrites are in accord with this trend, some samples display significant deviations to both higher and lower δ^{66}Zn values. The latter deviations are thought to relate to parent body rather than nebular processes, particularly volatile mobility induced by thermal or shock metamorphism (Luck et al., 2005; Moynier et al., 2011). As such, the

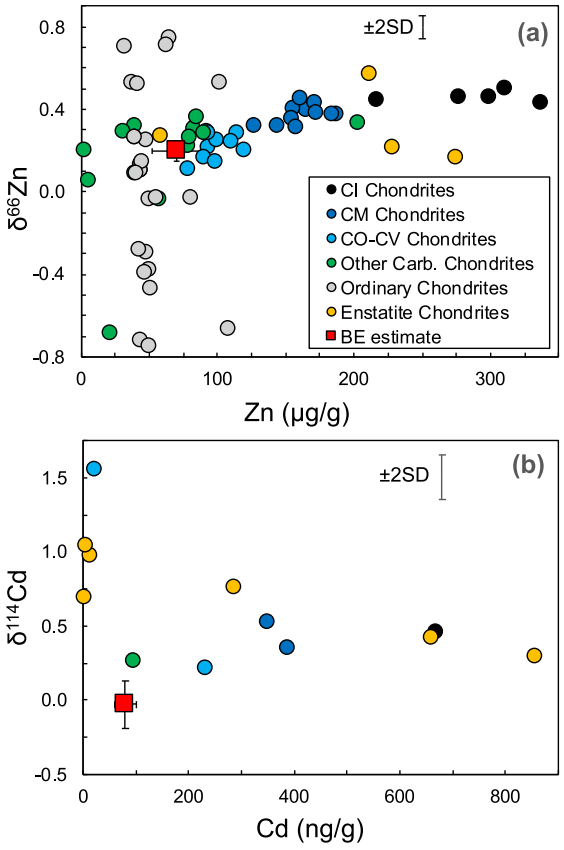

Fig. 4. Plots of (a) δ^{66}Zn versus Zn concentration and (b) δ^{114}Cd versus Cd concentration for chondritic meteorites and bulk Earth estimates. The estimated BE Zn and Cd concentrations are from Mahan et al. (2018) and Wang et al. (2018), respectively. The BE isotope compositions are based on the BSE values of the current study assuming no isotope fractionation during core segregation. Literature isotope data are from Luck et al. (2005), Moynier et al. (2011), Barrat et al. (2012), Sossi et al. (2015), Pringle et al. (2017), Mahan et al. (2018), Sossi et al. (2018), Creech & Moynier (2019) for Zn and from Baker et al. (2010) and Palk et al. (2018) for Cd (see Tables S7, S8 of Supplementary Material for details). The older Cd data for chondrites of Wombacher et al. (2003) and Wombacher et al. (2008) are not plotted due to large uncertainties.

trend defined by the majority of the carbonaceous chondrites has been interpreted to reflect processes in the protosolar disk, such as variable mixing of meteoritic components (Luck et al., 2005; Pringle et al., 2017).

Published results for Zn (Bridgestock et al., 2014; Mahan et al., 2017) demonstrate that isotope fractionation during metal-silicate partitioning, and hence core formation, is either negligible or nearly so. As such, the $\delta^{66}Zn_{BSE}$ value of 0.20 ± 0.05 ‰ is also directly relevant for the bulk Earth (BE). Using a BE Zn concentration of 70 ± 18 μg/g (Mahan et al. (2018), the BE plots along the volatile depleted end of the nebular Zn trend defined by carbonaceous chondrites (Fig. 4a), as previously shown by Sossi et al. (2018). This suggests that Earth's volatile inventory may well have been provided by material resembling carbonaceous and/or enstatite chondrites as well as bulk material from ordinary chondrite parent bodies. However, assuming that no further Zn isotope fractionation took place during accretion, the $\delta^{66}Zn$ value of the BSE and BE is not in accord with models which posit that volatiles were delivered to Earth solely by CI- or CM-like material, as there is a small but significant difference in the Zn isotope compositions of these chondrite groups compared to the BSE. Instead, Earth's Zn isotope signature closely resembles more volatile depleted CV and CO chondrites.

For Cd, the BE estimate uses a concentration of 80 ± 21 ng/g, which implies that the majority of the BE Cd inventory (~70 %) is concentrated in the core (Wang et al. (2018). It furthermore assumes that the Cd isotope compositions of the BE and BSE are identical, with $\delta^{114}Cd$ = –0.06 ± 0.03 ‰, due to lack of metal-silicate isotope fractionation during core formation (Fig. 4b). Whilst experimental evidence for the latter inference is currently lacking, the assumption is reasonable, given the absence of Zn isotope fractionation during metal-silicate partitioning. A 'nebular' trend, as defined for Zn by the data of carbonaceous chondrites in Fig. 4a is not clearly apparent in the Cd plot of Fig. 4b, due to the paucity of published high precision Cd isotope data for meteorites and the scatter in the available results. Furthermore, the Cd isotope compositions of meteorites are more readily altered by volatilisation than Zn isotopes and chondritic $\delta^{114}Cd$ values that fall outside the range of about 0.2 to 0.5 ‰ are thought to reflect isotope fractionation during parent body processing (Wombacher et al., 2003; Wombacher et al., 2008; Palk et al., 2018).

The data shown in Fig. 4b hence suggest that $\delta^{114}Cd_{BSE}$, and therefore the inferred $\delta^{114}Cd_{BE}$ value, are about 0.2 ‰ lower compared to the lightest Cd isotope compositions recorded for carbonaceous and enstatite chondrites. There are a number of reasonable explanations for this discrepancy. First, the limited currently available Cd isotope data for chondrites may be biased toward $\delta^{114}Cd$ values that are too high on average. Second, it is possible that Earth acquired its Cd inventory from chondritic meteorites but that subsequent processes fractionated the Cd isotope composition of the BE or BSE during accretion. Loss of Cd by volatilisation from an early terrestrial magma ocean or partial recondensation of volatilised Cd following the giant impact are, however, expected to generate an Earth with a heavy Cd isotope composition relative to chondrites. Volatility-related Cd isotope fractionations are hence unlikely to be responsible for the low $\delta^{114}Cd$ of the BSE. Fractionation of Cd isotopes during core formation provides a reasonable alternative mechanism, especially as a smaller fraction of the BE Cd inventory is inferred to be present in the BSE than for Zn, possibly due to late segregation of a sulphide melt to the core (O'Neill, 1991; Savage et al., 2015; Wang et al., 2018). Experimental evidence for Cd isotope fractionation during core formation, which confirms or rebuts this conclusion is not available at present, however. Finally, as suggested previously for Zn (Sossi et al., 2018), it is conceivable that the terrestrial budget of Cd was partly provided by material which had a lower $\delta^{114}Cd$ compared to the known compositions of carbonaceous and enstatite chondrites that are unaffected by metamorphic alteration. If correct, this may imply that a significant portion of Earth's Cd and other volatile elements may have been sourced from a reservoir that is not related to known carbonaceous and enstatite chondrites. However, considering the current uncertainties, the origin and significance of the observed offset in $\delta^{114}Cd$ between the BSE and carbonaceous and enstatite chondrites remains to be resolved by further investigations.

6. Conclusions

The Zn and Cd isotope compositions of a comprehensive suite of diverse terrestrial rocks were determined to constrain the extent of Zn and Cd isotope fractionation during magmatic processes and to better define the $\delta^{66}Zn$ and $\delta^{114}Cd$ values of the silicate Earth.

Results obtained for spinel lherzolites provide a $\delta^{114}Cd_{BSE}$ value of –0.06 ± 0.03 ‰ (2SD). For Zn, the lherzolite data of this study are combined with literature results to define a $\delta^{66}Zn_{BSE}$ value of +0.20 ± 0.05 ‰ (2SD), in accord with previous BSE estimates (Wang et al., 2017; Sossi et al., 2018). Data obtained for komatiites are in accord with the $\delta^{114}Cd_{BSE}$ and $\delta^{66}Zn_{BSE}$ estimates, which suggests that both mantle isotope compositions are broadly unchanged since the Archean. Analyses of loess as well as continental igneous rocks furthermore yield upper continental crust compositions of $\delta^{114}Cd$ = 0.03 ± 0.10 ‰ and $\delta^{66}Zn$ = 0.23 ± 0.07 ‰.

The Zn data available for peridotites and oceanic basalts define a mantle array, with basalts having higher Zn concentrations and higher $\delta^{66}Zn$ than the peridotites. These systematics imply that Zn is slightly incompatible during mantle melting and melt differentiation, with associated enrichment of heavy Zn isotopes in the melt phase. Cadmium is marginally more incompatible than Zn during partial mantle melting and MORB and OIB samples generally display minor enrichments of heavy Cd isotopes relative to peridotites. However, secondary processes including magmatic volatilisation, metasomatism and weathering can generate Cd isotope variability in both mantle melts and peridotites, obscuring the primary array produced by mantle melting.

The $\delta^{66}Zn_{BSE}$ estimates of this and previous studies resemble the Zn isotope compositions of CV and CO carbonaceous and some enstatite chondrites. Given the negligible Zn isotope fractionation during core formation, this overlap is consistent with delivery of Zn and other similarly volatile elements to Earth solely by material related to carbonaceous, enstatite and/or ordinary chondrites. Conversely, the BSE has a lower $\delta^{114}Cd$ value compared to known enstatite and carbonaceous chondrites. This implies that either the Cd isotope signature of the BSE was altered during accretion and/or core formation or that Earth accreted material with a Cd isotope composition that is not recorded in hitherto analysed carbonaceous and enstatite chondrites. Importantly, delivery of Zn and Cd solely by CI and CM chondrites is not in accord with the terrestrial stable isotope compositions of both elements.

Data availability

Data will be made available on request.

Declaration of Competing Interest

The authors declare that they have no known competing financial interests or personal relationships that could have appeared to influence the work reported in this paper.

Acknowledgements

Sincere thanks are extended to (in alphabetical order) Alex Halliday, Catherine Chauvel, Godfrey Fitton, Jeff Alt, Karsten Haase, Kevin Burton and Nick Arndt for providing invaluable samples which made this study possible. The manuscript profited immensely from comprehensive and constructive reviews by Paul Savage, Paolo Sossi, Frank Wombacher and editorial handling by Fred Moynier. The research was supported by STFC research grants to MR (ST/F002157/1), ST/J0012260/1) and STFC quota studentships to HR and EP.

Appendix A. Supplementary material

Supplementary Text: Extended Methods – Modelling trace element concentrations and stable isotope compositions for batch melting and fractional crystallisation. Estimation of D_{Zn}, D_{Cd} and $\Delta^{66}Zn_{mantle-melt}$, $\Delta^{114}Cd_{mantle-melt}$ values based on the Zn, Cd concentrations and isotope compositions of the BSE and continental crust. Supplementary Tables. Table S1 Column chemistry for the separation of Zn from silicate rock and meteorite samples. Table S2 Column chemistry for the separation of Cd from silicate rocks and meteorites. Table S3 Comparison of Zn isotope data for geological reference materials from this and previous studies. Table S4 Comparison of Cd isotope data for geological reference materials from this and previous studies. Table S5 Literature Zn isotope data used in Figures 1 and 2. Table S6 Literature Cd isotope data used in Figures 1 and 2. Table S7 Literature Zn isotope data for chondrites used in Figure 4. Table S8 Literature Cd isotope data for chondrites used in Figures 4. Supplementary material to this article can be found online at https://doi.org/10.1016/j.gca.2022.09.041.

References

Abouchami, W., Galer, S.J.G., Horner, T.J., Rehkämper, M., Wombacher, F., Xue, Z., Lambelet, M., Gault-Ringold, M., Stirling, C.H., Schönbächler, M., Shiel, A.E., Weis, D., Holdship, P.F., 2013. A common reference material for cadmium isotope studies - NIST SRM 3108. Geostand. Geoanal. Res. 37, 5–17.

Adam, J., Green, T., 2006. Trace element partitioning between mica- and amphibole-bearing garnet lherzolite and hydrous basanitic melt: 1. Experimental results and the investigation of controls on partitioning behaviour. Contrib. Mineral. Petrol. 152, 1–17.

Albarède, F., 2009. Volatile accretion history of the terrestrial planets and dynamic implications. Nature 461, 1227–1233.

Albarède, F., Ballhaus, C., Blichert-Toft, J., Lee, C.-T., Marty, B., Moynier, F., Yin, Q.-Z., 2013. Asteroidal impacts and the origin of terrestrial and lunar volatiles. Icarus 222, 44–52.

Allan, J.F., Dick, H.J.B., 1996. Cr-rich spinel as a tracer for melt migration and melt-wall rock interaction in the mantle: Hess Deep, Leg 147. Proc. ODP Sci. Res. 147, 157–172.

Anguelova, M., Fehr, M.A., Takazawa, E., Schönbächler, M., 2022. Titanium isotope heterogeneity in the Earth's mantle: a case study of the Horoman peridotite massif. Geochim. Cosmochim. Acta 335, 356–368.

Archer, C., Andersen, M.B., Cloquet, C., Conway, T.M., Dong, S., Ellwood, M., Moore, R., Nelson, J., Rehkämper, M., Rouxel, O., Samanta, M., Shin, K.-C., Sohrin, Y., Takano, S., Wasylenki, L., 2017. Inter-calibration of a proposed new primary reference standard AA-ETH Zn for zinc isotopic analysis. J. Anal. At. Spectrom. 32, 415–419.

Arndt, N.T., 1986. Differentiation of komatiite flows. J. Petrol. 27, 279–301.

Arnold, T., Schönbächler, M., Rehkämper, M., Dong, S., Zhao, F.-J., Kirk, G.J.D., Coles, B.J., Weiss, D.J., 2010. Measurement of zinc stable isotope ratios in biogeochemical matrices by double-spike MC-ICPMS and determination of the isotope ratio pool available for plants from soil. Anal. Bioanal. Chem. 398, 3115–3125.

Baker, R.G.A., Schönbächler, M., Rehkämper, M., Williams, H., Halliday, A.N., 2010. The thallium isotope composition of carbonaceous chondrites – new evidence for live ^{205}Pb in the early solar system. Earth Planet. Sci. Lett. 291, 39–47.

Ballhaus, C., Laurenz, V., Münker, C., Fonseca, R.O.C., Albarède, F., Rohrbach, A., Lagos, M., Schmidt, M.W., Jochum, K.-P., Stoll, B., Weis, U., Helmy, H.M., 2013. The U/Pb ratio of the Earth's mantle – A signature of late volatile addition. Earth Planet. Sci. Lett. 362, 237–245.

Barrat, J.A., Zanda, B., Moynier, F., Bollinger, C., Liorzou, C., Bayon, G., 2012. Geochemistry of CI chondrites: major and trace elements, and Cu and Zn isotopes. Geochim. Cosmochim. Acta 83, 79–92.

Barraza, F., Moore, R.E.T., Rehkämper, M., Schreck, E., Lefeuvre, G., Kreissig, K., Coles, B.J., Maurice, L., 2019. Cadmium isotope fractionation in the soil – cacao systems of Ecuador: a pilot field study. RSC Adv. 9, 34011–34022.

Bermingham, K.R., Worsham, E.A., Walker, R.J., 2018. New insights into Mo and Ru isotope variation in the nebula and terrestrial planet accretionary genetics. Earth Planet. Sci. Lett. 487, 221–229.

Beunon, H., Mattielli, N., Doucet, L.S., Moine, B., Debret, B., 2020. Mantle heterogeneity through Zn systematics in oceanic basalts: Evidence for a deep carbon cycling. Earth Sci. Rev. 205, 103174.

Bigalke, M., Weyer, S., Kobza, J., Wilcke, W., 2010. Stable Cu and Zn isotope ratios as tracers of sources and transport of Cu and Zn in contaminated soil. Geochim. Cosmochim. Acta 74, 6801–6813.

Boyet, M., Bouvier, A., Frossard, P., Hammouda, T., Garçon, M., Gannoun, A., 2018. Enstatite chondrites EL3 as building blocks for the Earth: The debate over the ^{146}Sm–^{142}Nd systematics. Earth Planet. Sci. Lett. 488, 68–78.

Braukmüller, N., Wombacher, F., Funk, C., Münker, C., 2019. Earth's volatile element depletion pattern inherited from a carbonaceous chondrite-like source. Nature Geosci. 12, 564–568.

Bridgestock, L.J., Williams, H., Rehkämper, M., Larner, F., Giscard, M.D., Hammond, S., Coles, B., Andreasen, R., Wood, B.J., Theis, K.J., Smith, C.L., Benedix, G.K., Schönbächler, M., 2014. Unlocking the zinc isotope systematics of iron meteorites. Earth Planet. Sci. Lett. 400, 153–164.

Burkhardt, C., Kleine, T., Oberli, F., Pack, A., Bourdon, B., Wieler, R., 2011. Molybdenum isotope anomalies in meteorites: Constraints on solar nebula evolution and origin of the Earth. Earth Planet. Sci. Lett. 312, 390–400.

Casey, J.F., 1997. Comparison of major- and trace-element geochemistry of abyssal peridotites and mafic plutonic rocks with basalts from the MARK region of the Mid-Atlantic Ridge. Proc. ODP Sci. Res. 153, 181–241.

Chauvel, C., Dupré, B., Arndt, N.T., 1993. Pb and Nd isotopic correlation in Belingwe komatiites and basalts. In: Bickle, M.J., Nisbet, E.G. (Eds.), the Geology of the Belingwe Greenstone Belt, Zimbabwe. A.A. Balkema, Rotterdam, pp. 167–174.

Chen, F.H., Bloemendal, J., Wang, J.M., Li, J.J., Oldfield, F., 1997. High-resolution multi-proxy climate records from Chinese loess: evidence for rapid climatic changes over the last 75 kyr. Palaeogeogr. Palaeoclimatol. Palaeoecol. 130, 323–335.

Chen, H., Savage, P.S., Teng, F.-Z., Helz, R.T., Moynier, F., 2013. Zinc isotope fractionation during magmatic differentiation and the isotopic composition of the bulk Earth. Earth Planet. Sci. Lett. 369–370, 34–42.

Corgne, A., Keshav, S., Wood, B.J., McDonough, W.F., Fei, Y., 2008. Metal–silicate partitioning and constraints on core composition and oxygen fugacity during Earth accretion. Geochim. Cosmochim. Acta 72, 574–589.

Creech, J.B., Moynier, F., 2019. Tin and zinc stable isotope characterisation of chondrites and implications for early Solar System evolution. Chem. Geol. 511, 81–90.

Dauphas, N., 2017. The isotopic nature of the Earth's accreting material through time. Nature 541, 521–524.

Dauphas, N., Teng, F.-Z., Arndt, N.T., 2010. Magnesium and iron isotopes in 2.7 Ga Alexo komatiites: Mantle signatures, no evidence for Soret diffusion, and identification of diffusive transport in zoned olivine. Geochim. Cosmochim. Acta 74, 3274–3291.

Davis, F.A., Humayun, M., Hirschmann, M.M., Cooper, R.S., 2013. Experimentally determined mineral/melt partitioning of first-row transition elements (FRTE) during partial melting of peridotite at 3GPa. Geochim. Cosmochim. Acta 104, 232–260.

Ding, Z.L., Xiong, S.F., Sun, J.M., Yang, S.L., Gu, Z.Y., Liu, T.S., 1999. Pedostratigraphy and paleomagnetism of a~ 7.0 Ma eolian loess–red clay sequence at Lingtai, Loess Plateau, north-central China and the implications for paleomonsoon evolution. Palaeogeogr. Palaeoclimatol. Palaeoecol. 152, 49–66.

Doucet, L.S., Mattielli, N., Ionov, D.A., Debouge, W., Golovin, A.V., 2016. Zn isotopic heterogeneity in the mantle: A melting control? Earth Planet. Sci. Lett. 451, 232–240.

Dupré, B., Chauvel, C., Arndt, N.T., 1984. Pb and Nd isotopic study of two Archean komatiitic flows from Alexo, Ontario. Geochim. Cosmochim. Acta 48, 1965–1972.

Edwards, S.J., Malpas, J., 1996. Melt-peridotite interactions in shallow mantle at the East Pacific Rise: evidence from ODP Site 895 (Hess Deep). Mineral. Mag. 60, 191–206.

Fischer-Gödde, M., Kleine, T., 2017. Ruthenium isotopic evidence for an inner Solar System origin of the late veneer. Nature 541, 525–527.

Fischer-Gödde, M., Elfers, B.-M., Münker, C., Szilas, K., Maier, W.D., Messling, N., Morishita, T., Van Kranendonk, M., Smithies, H., 2020. Ruthenium isotope vestige of Earth's pre-late-veneer mantle preserved in Archaean rocks. Nature 579, 240–244.

Gallet, S., Jahn, B.-M., Van Vliet Lanoë, B., Dia, A., Rossello, E., 1998. Loess geochemistry and its implications for particle origin and composition of the upper continental crust. Earth Planet. Sci. Lett. 156, 157–172.

Gillmann, C., Golabek, G.J., Raymond, S.N., Schönbächler, M., Tackley, P., Dehant, V., Debaille, V., 2020. Dry late accretion inferred from Venus's coupled atmosphere and internal evolution. Nat. Geosci. 13, 265–269.

Herzog, G.F., Moynier, F., Albarède, F., Berezhnoy, A.A., 2009. Isotopic and elemental abundances of copper and zinc in lunar samples, Zagami, Pele's hairs, and a terrestrial basalt. Geochim. Cosmochim. Acta 73, 5884–5904.

Hinkley, T.K., Le Cloarec, M.-F., Lambert, G., 1994. Fractionation of families of major, minor, and trace metals across the melt-vapor interface in volcanic exhalations. Geochim. Cosmochim. Acta 58, 3255–3263.
Hofmann, A.W., 2014. Sampling mantle heterogeneity through oceanic basalts: isotopes and trace elements. In: Holland, H.D., Turekian, K.K. (Eds.), Treatise on Geochemistry. 2nd edn. Elsevier, Amsterdam, pp. 67–101.
Holzheid, A., Sylvester, P., O'Neill, H.S.C., Rubie, D.C., Palme, H., 2000. Evidence for a late chondritic veneer in the Earth's mantle from high-pressure partitioning of palladium and platinum. Nature 406, 396–399.
Horn, I., Foley, S.F., Jackson, S.E., Jenner, G.A., 1994. Experimentally determined partitioning of high field strength-and selected transition elements between spinel and basaltic melt. Chem. Geol. 117, 193–218.
Huang, J., Chen, S., Zhang, X.C., Huang, F., 2018a. Effects of melt percolation on Zn isotope heterogeneity in the mantle: constraints from peridotite massifs in Ivrea-Verbano Zone, Italian Alps. J. Geophys. Res. 123, 2706–2722.
Huang, J., Zhang, X.-C., Chen, S., Tang, L., Wörner, G., Yu, H., Huang, F., 2018b. Zinc isotopic systematics of Kamchatka-Aleutian arc magmas controlled by mantle melting. Geochim. Cosmochim. Acta 238, 85–101.
Huang, J., Ackerman, L., Zhang, X.C., Huang, F., 2019. Mantle Zn isotopic heterogeneity caused by melt-rock reaction: evidence from Fe-rich peridotites and pyroxenites from the Bohemian Massif, Central Europe. J. Geophys. Res. 124, 3588–3604.
Imseng, M., Wiggenhauser, M., Keller, A., Müller, M., Rehkämper, M., Murphy, K., Kreissig, K., Frossard, E., Wilcke, W., Bigalke, M., 2018. Fate of Cd in agricultural soils: a stable isotope approach to anthropogenic impact, soil formation, and soil-plant cycling. Environ. Sci. Technol. 52, 1919–1928.
Irving, A.J., 1980. Petrology and geochemistry of composite ultramafic xenoliths in alkalic basalts and implications for magmatic processes within the mantle. Am. J. Sci. 280-A, 389–426.
Javoy, M., Kaminski, E., Guyot, F., Andrault, D., Sanloup, C., Moreira, M., Labrosse, S., Jambon, A., Agrinier, P., Davaille, A., Jaupart, C., 2010. The chemical composition of the Earth: Enstatite chondrite models. Earth Planet. Sci. Lett. 293, 259–268.
Jochum, K.P., Arndt, N.T., Hofmann, A.W., 1991. Nb-Th-La in komatiites and basalts: constraints on komatiite petrogenesis and mantle evolution. Earth Planet. Sci. Lett. 107, 272–289.
Kiseeva, E.S., Wood, B.J., 2013. A simple model for chalcophile element partitioning between sulphide and silicate liquids with geochemical applications. Earth Planet. Sci. Lett. 383, 68–81.
Kruckenberg, S.C., Tikoff, B., Toy, V.G., Newman, J., Young, L.I., 2013. Strain localization associated with channelized melt migration in upper mantle lithosphere: Insights from the Twin Sisters ultramafic complex, Washington, USA. J. Struct. Geol. 50, 133–147.
Lahaye, Y., Arndt, N., 1996. Alteration of a komatiite flow from Alexo, Ontario, Canada. J. Petrol. 37, 1261–1284.
Larner, F., Rehkämper, M., 2012. Evaluation of stable isotope tracing for ZnO nanomaterials–new constraints from high precision isotope analyses and modeling. Environ. Sci. Technol. 46, 4149–4158.
Le Roux, V., Dasgupta, R., Lee, C.-T.-A., 2011. Mineralogical heterogeneities in the Earth's mantle: Constraints from Mn Co, Ni and Zn partitioning during partial melting. Earth Planet. Sci. Lett. 307, 395–408.
Lee, D.-C., Halliday, A.N., Davies, G.R., Essene, E.J., Fitton, J.G., Temdjim, R., 1996. Melt enrichment of shallow depleted mantle: a detailed petrological, trace element and isotopic study of mantle-derived xenoliths and megacrysts from the Cameroon Line. J. Petrol. 37, 415–441.
Li, Y., Audétat, A., 2012. Partitioning of V, Mn Co, Ni, Cu, Zn, As, Mo, Ag, Sn, Sb, W, Au, Pb, and Bi between sulfide phases and hydrous basanite melt at upper mantle conditions. Earth Planet. Sci. Lett. 355–356, 327–340.
Liao, R., Zhu, H., Deng, J., Zhang, L., Li, H., Li, C., Liu, H., Sun, W., 2020. Zinc isotopic systematics of the South China Sea basalts and implications for its behavior during plate subduction. Chem. Geol. 541, 119582.
Little, S.H., Vance, D., McManus, J., Severmann, S., 2016. Key role of continental margin sediments in the oceanic mass balance of Zn and Zn isotopes. Geology 44, 207–210.
Little, S.H., Munson, S., Prytulak, J., Coles, B.J., Hammond, S.J., Widdowson, M., 2019. Cu and Zn isotope fractionation during extreme chemical weathering. Geochim. Cosmochim. Acta 263, 85–107.
Liu, S.-A., Wang, Z.-Z., Li, S.-G., Huang, J., Yang, W., 2016. Zinc isotope evidence for a large-scale carbonated mantle beneath eastern China. Earth Planet. Sci. Lett. 444, 169–178.
Liu, M.S., Zhang, Q., Zhang, Y., Zhang, Z., Huang, F., Yu, H.M., 2019. High-precision Cd isotope measurements of soil and rock reference materials by MC-ICP-MS with double spike correction. Geostand. Geoanal. Res. 44, 169–182.
Luck, J.-M., Ben, O.D., Albarède, F., 2005. Zn and Cu isotopic variations in chondrites and iron meteorites: Early solar nebula reservoirs and parent-body processes. Geochim. Cosmochim. Acta 69, 5351–5363.
MacKenzie, J.M., Canil, D., 2008. Volatile heavy metal mobility in silicate liquids: Implications for volcanic degassing and eruption prediction. Earth Planet. Sci. Lett. 269, 488–496.
Mahan, B., Siebert, J., Pringle, E.A., Moynier, F., 2017. Elemental partitioning and isotopic fractionation of Zn between metal and silicate and geochemical estimation of the S content of the Earth's core. Geochim. Cosmochim. Acta 196, 252–270.
Mahan, B., Siebert, J., Blanchard, I., Borensztajn, S., Badro, J., Moynier, F., 2018. Constraining compositional proxies for Earth's accretion and core formation through high pressure and high temperature Zn and S metal-silicate partitioning. Geochim. Cosmochim. Acta 235, 21–40.
Marty, B., 2012. The origins and concentrations of water, carbon, nitrogen and noble gases on Earth. Earth Planet. Sci. Lett. 313–314, 56–66.
Mattielli, N., Haenecour, P., Debaille, V., 2012. Zn isotope fractionation in Archean komatiites and associated lava-flows. Mineral. Mag. 76, 2080.
McCoy-West, A.J., Fitton, J.G., Pons, M.-L., Inglis, E.C., Williams, H.M., 2018. The Fe and Zn isotope composition of deep mantle source regions: Insights from Baffin Island picrites. Geochim. Cosmochim. Acta 238, 542–562.
McDonough, W.F., Sun, S.-S., 1995. The composition of the Earth. Chem. Geol. 120, 223–253.
Moore, R.E.T., Larner, F., Coles, B.J., Rehkämper, M., 2017. High precision zinc stable isotope measurement of certified biological reference materials using the double spike technique and multiple collector-ICP-MS. Anal. Bioanal. Chem. 409, 2941–2950.
Moynier, F., Paniello, R.C., Gounelle, M., Albarède, F., Beck, P., Podosek, F., Zanda, B., 2011. Nature of volatile depletion and genetic relationships in enstatite chondrites and aubrites inferred from Zn isotopes. Geochim. Cosmochim. Acta 75, 297–307.
Murphy, K., Rehkämper, M., Kreissig, K., Coles, B., van de Flierdt, T., 2016. Improvements in Cd stable isotope analysis achieved through use of liquid-liquid extraction to remove organic residues from Cd separates obtained by extraction chromatography. J. Anal. At. Spectrom. 31, 319–327.
Niida, K., 1997. Mineralogy of MARK peridotites: replacement through magma chaneling examined from Hole 920D, MARK area. Proc. ODP, Sci. Results 153, 265–275.
Nisbet, E.G., Arndt, N.T., Bickle, M.J., Cameron, W.E., Chauvel, C., Cheadle, M., Hegner, E., Kyser, T.K., Martin, A., Renner, R., Roedder, E., 1987. Uniquely fresh 2.7 Ga komatiites from the Belingwe greenstone belt, Zimbabwe. Geology 15, 1147–1150.
Norman, M.D., Garcia, M.O., Bennett, V.C., 2004. Rhenium and chalcophile elements in basaltic glasses from Ko'olau and Moloka'i volcanoes: Magmatic outgassing and composition of the Hawaiian plume. Geochim. Cosmochim. Acta 68, 3761–3777.
Norris, C.A., Wood, B.J., 2017. Earth's volatile contents established by melting and vaporization. Nature 549, 507–510.
O'Neill, H.S.C., 1991. The origin of the Moon and the early history of the Earth – A chemical model. Part 2: The Earth. Geochim. Cosmochim. Acta 55, 1159–1172.
Opfergelt, S., Cornélis, J.T., Houben, D., Givron, C., Burton, K.W., Mattielli, N., 2017. The influence of weathering and soil organic matter on Zn isotopes in soils. Chem. Geol. 466, 140–148.
O'Reilly, S.Y., Griffin, W.L., Ryan, C.G., 1991. Residence of trace elements in metasomatized spinel lherzolite xenoliths: a proton-microprobe study. Contrib. Mineral. Petrol. 109, 98–113.
Palk, E., Andreasen, R., Rehkämper, M., Stunt, A., Kreissig, K., Coles, B., Schönbächler, M., Smith, C., 2018. Variable Tl, Pb, and Cd concentrations and isotope compositions of enstatite and ordinary chondrites-Evidence for volatile element mobilization and decay of extinct ^{205}Pb. Meteorit. Planet. Sci. 53, 167–186.
Palme, H., O'Neill, H.S.C., 2014. Cosmochemical estimates of mantle composition. In: Holland, H.D., Turekian, K.K. (Eds.), Treatise on Geochemistry Vol. 3, 2nd edn. Elsevier, Amsterdam, pp. 1–39.
Palme, H., Lodders, K., Jones, A., 2014. Solar System abundances of the elements. In: Holland, H.D., Turekian, K.K. (Eds.), Treatise on Geochemistry, vol. 2, 2nd edn. Elsevier, Amsterdam. pp. 15–36.
Peucker-Ehrenbrink, B., Jahn, B., 2001. Rhenium-osmium isotope systematics and platinum group element concentrations: Loess and the upper continental crust. Geochem. Geophys. Geosystems 2. 2001GC000172.
Piani, L., Marrocchi, Y., Rigaudier, T., Vacher, L.G., Thomassin, D., Marty, B., 2020. Earth's water may have been inherited from material similar to enstatite chondrite meteorites. Science 369, 1110–1113.
Pringle, E.A., Moynier, F., Beck, P., Paniello, R., Hezel, D.C., 2017. The origin of volatile element depletion in early solar system material: Clues from Zn isotopes in chondrules. Earth Planet. Sci. Lett. 468, 62–71.
Prytulak, J., Nielsen, S.G., Plank, T., Barker, M., Elliott, T., 2013. Assessing the utility of thallium and thallium isotopes for tracing subduction zone inputs to the Mariana arc. Chem. Geol. 345, 139–149.
Puchtel, I., Humayun, M., 2000. Platinum group elements in Kostomuksha komatiites and basalts: Implications for oceanic crust recycling and core-mantle interaction. Geochim. Cosmochim. Acta 64, 4227–4242.
Rehkämper, M., Halliday, A.N., Alt, J., Fitton, J.G., Zipfel, J., Takazawa, E., 1999a. Non-chondritic platinum-group element ratios in oceanic mantle lithosphere: petrogenetic signature of melt percolation? Earth Planet. Sci. Lett. 172, 65–81.
Rehkämper, M., Halliday, A.N., Fitton, J.G., Lee, D.-C., Wieneke, M., Arndt, N.T., 1999b. Ir, Ru, Pt, and Pd in basalts and komatiites: new constraints for the geochemical behavior of the platinum-group elements in the mantle. Geochim. Cosmochim. Acta 63, 3915–3934.
Rehkämper, M., Wombacher, F., Horner, T.J., Xue, Z., 2011. Natural and anthropogenic Cd isotope variations. In: Baskaran, M. (Ed.), Handbook of Environmental Isotope Geochemistry. Springer, Heidelberg, London, pp. 125–154.
Ripperger, S., Rehkämper, M., 2007. Precise determination of cadmium isotope fractionation in seawater by double spike MC-ICPMS. Geochim. Cosmochim. Acta 71, 631–642.
Rubin, K., 1997. Degassing of metals and metalloids from erupting seamount and mid-ocean ridge volcanoes: observations and predictions. Geochim. Cosmochim. Acta 61, 3525–3542.

Rudnick, R.L., Gao, S., 2014. Composition of the continental crust. In: Holland, H.D., Turekian, K.K. (Eds.), Treatise on Geochemistry. 2nd edn. Elsevier, Amsterdam, pp. 1–51.
Salters, V.J.M., Stracke, A., 2004. Composition of the depleted mantle. Geochem. Geophys. Geosys. 5, Q05B07.
Savage, P.S., Moynier, F., Chen, H., Shofner, G., Siebert, J., Badro, J., Puchtel, I.S., 2015. Copper isotope evidence for large-scale sulphide fractionation during Earth's differentiation. Geochem. Perspect. Lett. 1, 53–64.
Schmitt, A.-D., Galer, S.J.G., Abouchami, W., 2009. Mass-dependent cadmium isotopic variations in nature with emphasis on the marine environment. Earth Planet. Sci. Lett. 277, 262–272.
Schönbächler, M., Carlson, R.W., Horan, M.F., Mock, T.D., Hauri, E.H., 2010. Heterogeneous accretion and the moderately volatile element budget of Earth. Science 328, 884–887.
Siebert, J., Corgne, A., Ryerson, F.J., 2011. Systematics of metal–silicate partitioning for many siderophile elements applied to Earth's core formation. Geochim. Cosmochim. Acta 75, 1451–1489.
Sossi, P.A., Halverson, G.P., Nebel, O., Eggins, S.M., 2015. Combined separation of Cu, Fe and Zn from rock matrices and improved analytical protocols for stable isotope determination. Geostand. Geoanal. Res. 39, 129–149.
Sossi, P.A., Nebel, O., O'Neill, H.S.C., Moynier, F., 2018. Zinc isotope composition of the Earth and its behaviour during planetary accretion. Chem. Geol. 477, 73–84.
Sossi, P.A., Klemme, S., O'Neill, H.S.C., Berndt, J., Moynier, F., 2019. Evaporation of moderately volatile elements from silicate melts: experiments and theory. Geochim. Cosmochim. Acta 260, 204–231.
Takazawa, E., Frey, F.A., Shimizu, N., Obata, M., Bodinier, J.L., 1992. Geochemical evidence for melt migration and reaction in the upper mantle. Nature 359, 55–58.
Takazawa, E., Frey, F., Shimizu, N., Obata, M., 1996. Evolution of the Horoman peridotite (Hokkaido, Japan): Implications from pyroxene compositions. Chem. Geol. 134, 3–26.
Taylor, S.R., McLennan, S.M., 1985. The Continental Crust: Its Composition and Evolution. Blackwell Scientific, Oxford.
Taylor, S.R., McLennan, S.M., McCulloch, M.T., 1983. Geochemistry of loess, continental crustal composition and crustal model ages. Geochim. Cosmochim. Acta 47, 1897–1905.
Telus, M., Dauphas, N., Moynier, F., Tissot, F.L.H., Teng, F.-Z., Nabelek, P.I., Craddock, P.R., Groat, L.A., 2012. Iron, zinc, magnesium and uranium isotopic fractionation during continental crust differentiation: The tale from migmatites, granitoids, and pegmatites. Geochim. Cosmochim. Acta 97, 247–265.
Wade, J., Wood, B.J., 2005. Core formation and the oxidation state of the Earth. Earth Planet. Sci. Lett. 236, 78–95.
Walker, R.J., 2009. Highly siderophile elements in the Earth, Moon and Mars: update and implications for planetary accretion and differentiation. Chem. Erde Geochem. 69, 101–125.
Wang, Z., Becker, H., 2013. Ratios of S, Se and Te in the silicate Earth require a volatile-rich late veneer. Nature 499, 328–331.
Wang, H.S., Lineweaver, C.H., Ireland, T.R., 2018. The elemental abundances (with uncertainties) of the most Earth-like planet. Icarus 299, 460–474.
Wang, Z.-Z., Liu, S.-A., Liu, J., Huang, J., Xiao, Y., Chu, Z.-Y., Zhao, X.-M., Tang, L., 2017. Zinc isotope fractionation during mantle melting and constraints on the Zn isotope composition of Earth's upper mantle. Geochim. Cosmochim. Acta 198, 151–167.
Wänke, H., Dreibus, G., Jagoutz, E., 1984. Mantle chemistry and accretion history of the Earth. In: Kröner, A., Hanson, G.N., Goodwin, A.M. (Eds.), Archaean Geochemistry. Springer, Berlin, Heidelberg, pp. 1–24.
Warren, P.H., 2011. Stable-isotopic anomalies and the accretionary assemblage of the Earth and Mars: A subordinate role for carbonaceous chondrites. Earth Planet. Sci. Lett. 311, 93–100.
Wasson, J.T., Chou, C.L., 1974. Fractionation of moderately volatile elements in ordinary chondrites. Meteorit. Planet. Sci. 9, 69–84.
Wasson, J.T., Kallemeyn, G.W., 1988. Compositions of chondrites. Phil. Trans. R. Soc. Lond. Ser. A 325, 535–544.
Witt-Eickschen, G., Palme, H., O'Neill, H.S.C., Allen, C.M., 2009. The geochemistry of the volatile trace elements As, Cd, Ga, In and Sn in the Earth's mantle: New evidence from in situ analyses of mantle xenoliths. Geochim. Cosmochim. Acta 73, 1755–1778.
Wombacher, F., Rehkämper, M., Mezger, K., Münker, C., 2003. Stable isotope compositions of cadmium in geological materials and meteorites determined by multiple-collector ICPMS. Geochim. Cosmochim. Acta 67, 4639–4654.
Wombacher, F., Rehkämper, M., Mezger, K., Bischoff, A., Münker, C., 2008. Cadmium stable isotope cosmochemistry. Geochim. Cosmochim. Acta 72, 646–667.
Wood, B.J., Halliday, A.N., Rehkämper, M., 2010. Volatile accretion history of the Earth. Nature 467, E6–E7.
Wood, B.J., Smythe, D.J., Harrison, T., 2019. The condensation temperatures of the elements: A reappraisal. Am. Mineral. 104, 844–856.
Xue, Z., Rehkämper, M., Schönbächler, M., Statham, P.J., Coles, B.J., 2012. A new methodology for precise cadmium isotope analyses of seawater. Anal. Bioanal. Chem. 402, 883–893.
Yi, W., Halliday, A.N., Alt, J.C., Lee, D.-C., Rehkämper, M., Garcia, M.O., Langmuir, C.H., Su, Y., 2000. Cadmium, indium, tin, tellurium, and sulfur in oceanic basalrs: Implications for chalcophile element fractionation in the Earth. J. Geophys. Res. 105, 18927–18948.
Yoshikawa, M., Nakamura, E., 2000. Geochemical evolution of the Horoman peridotite complex: Implications for melt extraction, metasomatism, and compositional layering in the mantle. J. Geophys. Res. 105, 2879–2901.
Young, E.D., Kohl, I.E., Warren, P.H., Rubie, D.C., Jacobson, S.A., Morbidelli, A., 2016. Oxygen isotopic evidence for vigorous mixing during the Moon-forming giant impact. Science 351, 493–496.
Zelenski, M., Simakin, A., Taran, Y., Kamenetsky, V.S., Malik, N., 2021. Partitioning of elements between high-temperature, low-density aqueous fluid and silicate melt as derived from volcanic gas geochemistry. Geochim. Cosmochim. Acta 295, 112–134.
Zhang, G., Liu, Y., Moynier, F., Zhu, Y., Wang, Z., Hu, Z., Zhang, L., Li, M., Chen, H., 2020. Zinc isotopic composition of the lower continental crust estimated from lower crustal xenoliths and granulite terrains. Geochim. Cosmochim. Acta 276, 92–108.
Zhu, Y., Liu, Y., Xu, R., Moynier, F., Li, M., Chen, H., 2021. Deciphering the origin of a basanite-alkali basalt-tholeiite suite using Zn isotopes. Chem. Geol. 585, 120585.